Airplane signals in the Radio Neutrino Observatory in Greenland (RNO-G)

Bachelor's Thesis in Physics

Presented by
Oliver Schlemper
20.09.2024

Erlangen Centre for Astroparticle Physics
Friedrich-Alexander-Universität Erlangen-Nürnberg

Supervisor: Prof. Dr. Anna Nelles

Contents

1 Introduction

Since the proposal of the neutrino in a letter from Wolfgang Pauli in 1930, we have learned a lot about these fascinating particles. A lot of experiments were conducted in order to shape our understanding of the neutrino. Today we know that it does not carry electrical charge, therefore it is not deflected by magnetic fields. It interacts only weakly and its mass is so small only an upper bound could be determined experimentally [4]. These are the properties that make the neutrino especially interesting as a messenger particle in multi−messenger−astronomy. Unlike photons and cosmic rays, neutrinos do not get deflected on their trajectory through space and therefore point straight back to their origin. Measuring Ultra−High−Energy (UHE) neutrinos and reconstructing their arrival direction entails the possibility of identifying UHE phenomena in our universe. Studying those might help shaping the understanding of processes in our world.
The detection of UHE neutrinos however is non trivial. Due to their small cross section and vanishingly small flux, huge detector volumes are needed in order to be able to detect such a particle in a reasonable amount of time. The Radio Neutrino Observatory in Greenland (RNO-G) [3] aims to detect neutrinos in an energy range from 10 PeV to 100 EeV. It will measure radio signals originating from the Askaryan effect, that takes place when an UHE neutrino interacts with a dense medium. As detector medium RNO-G utilizes the natural abundant ice layer in Greenland. 35 stations, each consisting of 24 antennas, will be placed in a grid to cover a huge volume. The antennas and their positions were chosen in a way that makes direction reconstruction in case of a neutrino event possible. RNO-G is sensitive to signals in a frequency range from $\sim$ 80 MHz to $\sim$ 750 MHz. Although RNO-G is placed in a remote location there is still a huge background of diverse signals that get measured by the antennas. These backgrounds do potentially interfere with neutrino analysis. Besides non−anthropogenic backgrounds like wind, solar flares and thermal noise, human made signals can be found in the data. One of them is signals from airplanes that fly over RNO-G. As [1] has shown, it is possible to tag signals from airplanes in a radio neutrino detector and even utilize them for calibration. Airplane tagging therefore is one of the challenges at RNO-G.

In this thesis the abundance of airplanes and methods of identifying and tagging airplane signals at RNO-G are investigated. If used for calibration, it is necessary to know where, when and how often airplanes fly over RNO-G. It is also of great importance to know how far RNO-G can detect airplanes. When publishing results of neutrino or solar flare analysis one does want to avoid false results, due to airplane traffic, under all circumstances. An automatic tagging of periods with air traffic can help with the analysis.

Therefore, RNO-G is introduced in section 2. An overview of airtraffic around RNO-G is given in section 3. The methods that were used in order to analyze events measured by RNO-G are discussed in section 4. In section 5 the potential decline in trigger−rate with rising distance of airplanes was analysed, trying to identify the critical area, where airplanes might deposit signals in the detector. A short summary is given in section 6. A conclusion is given in section 7 and potential future work is discussed in section 8.

2 Radio Neutrino Observatory in Greenland (RNO-G)

In this section the Radio Neutrino Observatory in Greenland (RNO-G) [3] is presented. The in−ice radio neutrino detection method will be explained. Known backgrounds are listed and discussed. The basic structure of the instrument and the process of taking data are presented. Finally the flight tracker, the key part that makes airplane detection at RNO-G possible, is described.

2.1 Radio neutrino detection

UHE neutrinos at RNO-G will be detected with the Askaryan effect [3], the dominant effect for radio emission in ice. If an UHE neutrino interacts with a medium (ice) it produces a shower of secondary particles. Those particles travel through the medium faster than the speed of light in that medium. There are three main effects that lead to an excess of negatively charged particles (electrons) in the shower front. Namely positron annihilation and dragging of Compton and $\delta-$electrons into the shower. This uncompensated moving charge leads to Cherenkov emission in the radio regime. This emission is coherent close to the Cherenkov cone, resulting in a strong signal close to the cone. This effect was proposed by G. A. Askaryan in the 1960s [5].
The neutrino flux above 10 PeV is rather small [3]. Therefore huge effective detector volumes are needed in order to detect such interactions within reasonable time. Greenland has a natural abundance of thick layers of ice, that meet the criteria for density and radio opacity for building a low cost radio neutrino detector. The attenuation length of radio waves in ice is ~ 1 km, making it possible to construct huge detector volumes with a sparse arrangement of detector stations. A single station consists of several radio antennas, arranged in such a way that neutrino event reconstruction is made possible. The exact layout will be discussed in section 2.2.

2.2 Layout

The RNO-G array is located at Summit Station in Greenland ($72°35'46''$ N, $38°25'19''$ W). Once finished it will consist of 35 stations, placed in a grid, each roughly 1 km apart. In 2021, 3 stations (11, 21, 22) were deployed, joined by 4 more stations (12, 13, 23, 24) in 2022, which are currently running and taking data.

Each station consists of 24 antennas, also referred to as channels. 9 antennas (LPDAs) are placed just below the ice surface, separated into 3 arms parallel to the ground. Each arm contains 1 upward and 2 diagonally downward facing antennas. That makes a total of 3 upward facing antennas. As RNO-G tries to detect neutrino interactions in the ice, all signals coming from above can be considered as background to neutrino searches. The upward facing antennas are used to veto those events. The other 15 antennas are divided up into 3 strings that go down into the ice. The power string holds a total of 9 antennas, 2 of them being horizontally polarized (Hpol) and the others being vertically polarized (Vpol). The antennas are positioned at different heights, reaching down to 100 m. Finally there are 2 support strings each containing 2 Vpol and 1 Hpol antennas. The Vpol antennas will be used for vertex and signal arrival direction reconstruction. Combined with the Hpol antennas the polarisation of

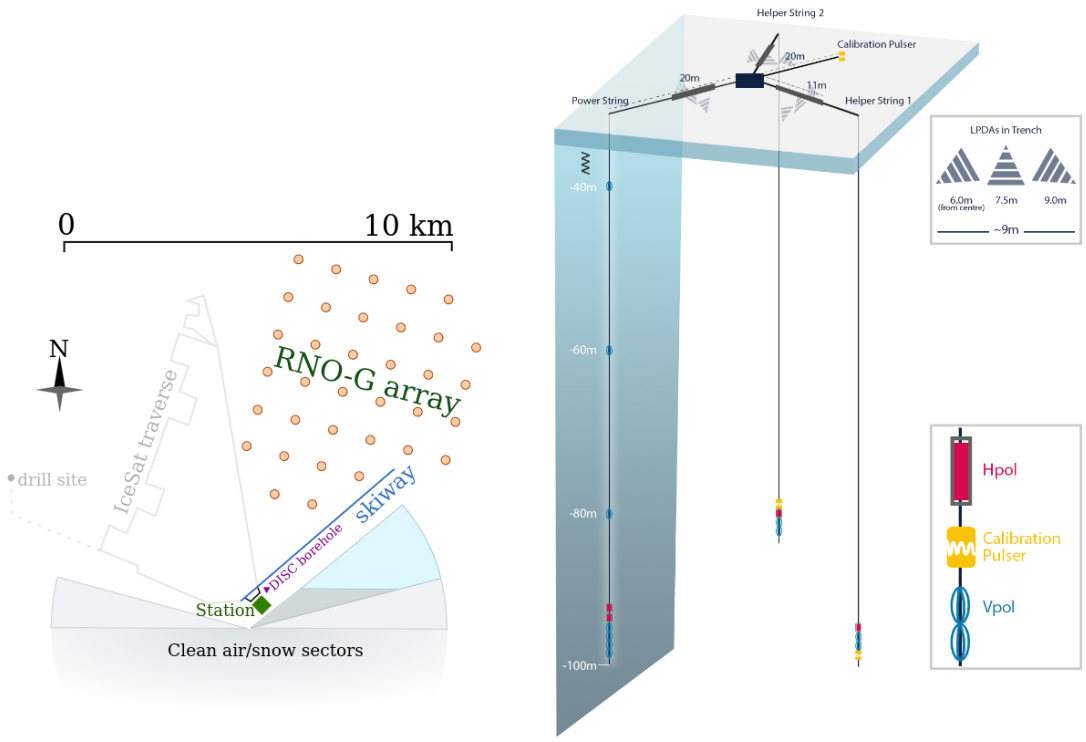

Figure 1: Left: Planned setup for RNO-G [3]. The array is shown from above. Every point in the figure represents a single station.
Right: Single station setup in RNO-G. Each station constists of 24 antennas. 9 LPDAs are burried right below the surface. The station is divided in 3 strings. The power string holds a total of 9 antennas at different heights in the ice. The support strings hold 3 antennas each. Each string has a calibration pulser. Vpol and Hpol antennas have vertical and horizontal polarisation.

the electric field and neutrino arrival direction can be reconstructed.

2.3 Triggers and saved data

Storing a continous stream of data from all antennas in RNO-G would lead to a huge amount of data and would consume a lot of power. Every station at RNO-G produces its own energy via 2 solar panels, storing 5 kWh of Energy (3 days of operation at full capacity (24W)) in a lead battery to ensure functionality at night. Although not in the initial design, wind turbines are tested to supply RNO-G stations with energy. This leads to an effective downtime of the whole array in winter and during times without sun (wind). Still the stations have to be designed to function very energy efficient. The received signal from the antennas is fed into a chain of hardware components where the signal gets amplified and filtered. The 9 LPDAs are connected to the SURFACE board. The antennas deep down are connected to a combination of the IGLU board (In-ice Gain with Low-power Unit) and the DRAB board (Down-hole Receiver and Amplifier Board). Due to the amplification, the signal passes through an effective band pass

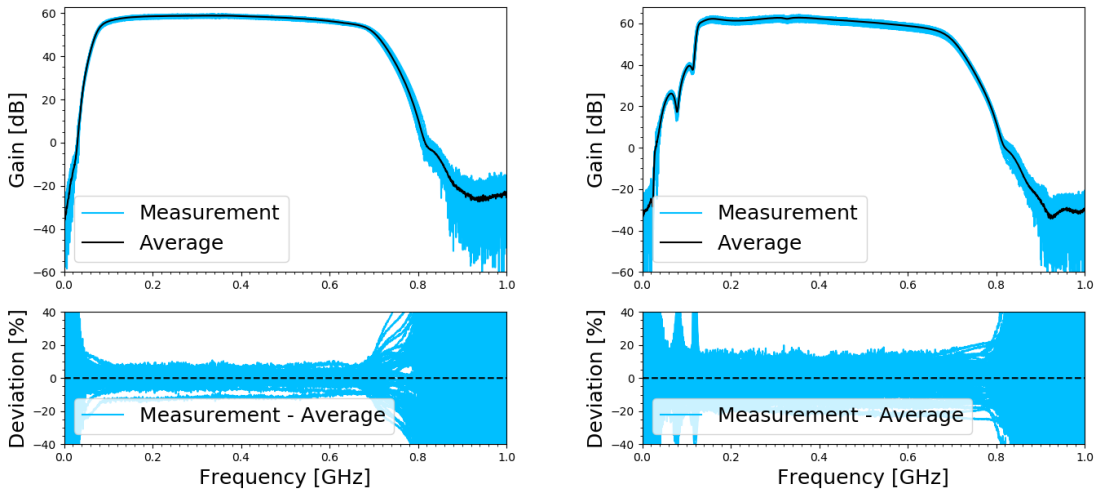

Figure 2: Gain of the RNO-G amplifiers. Left: 12 SURFACE amplifiers. Right: Combination of 23 IGLU and DRAB amplifiers, including a 50 m optical fiber cable. The amplification of both setups is shown as a function of the frequency. Figure is taken from [3]

filter, where it gets filtered for frequencies from $\sim$ 80 MHz to $\sim$ 750 MHz. To ensure that power intensive digitisation of data only happens if needed, this process has to be triggered. Triggering is based on the envelope of a signal, which gets constructed with hardware components. It is is less susceptible to noise. There are 3 different types of triggers [13]:

- **Deep trigger** (low threshold trigger):
  If 2 out of 4 channels in the phased array exceed a certain threshold coincidentally (30 ns) an event gets triggered.

- **Shallow trigger** (radiant trigger):
  A shallow event is triggered if either 2 out of 6 diagonally downward or 2 out of 3 upward facing antennas exceed a certain threshold in a coincidence window of 50 ns.

- **Force trigger**:
  A so called force trigger triggers every 10 seconds regardless of the voltage at the antennas, in order to study the noise environment.

The thresholds are continuously adjusted to achieve a target trigger rate in every station. Therefore thresholds can vary across different stations. All stations trigger independently from another. When triggering 2048 samples get stored with a sampling frequency of 3.2 GHz. Therefore the last 640 ns get saved. Those 2048 samples are called an event and the amplitude [V] over time is called the trace of the signal. The events get stored in so called runs. A normal run is usually 2h long. There are also test and calibration runs. Every event in RNO-G can be uniquely identified by its station number, run number and event number. When analysing signals one usually does also want to see its frequency components. They can be obtained by the Fourier

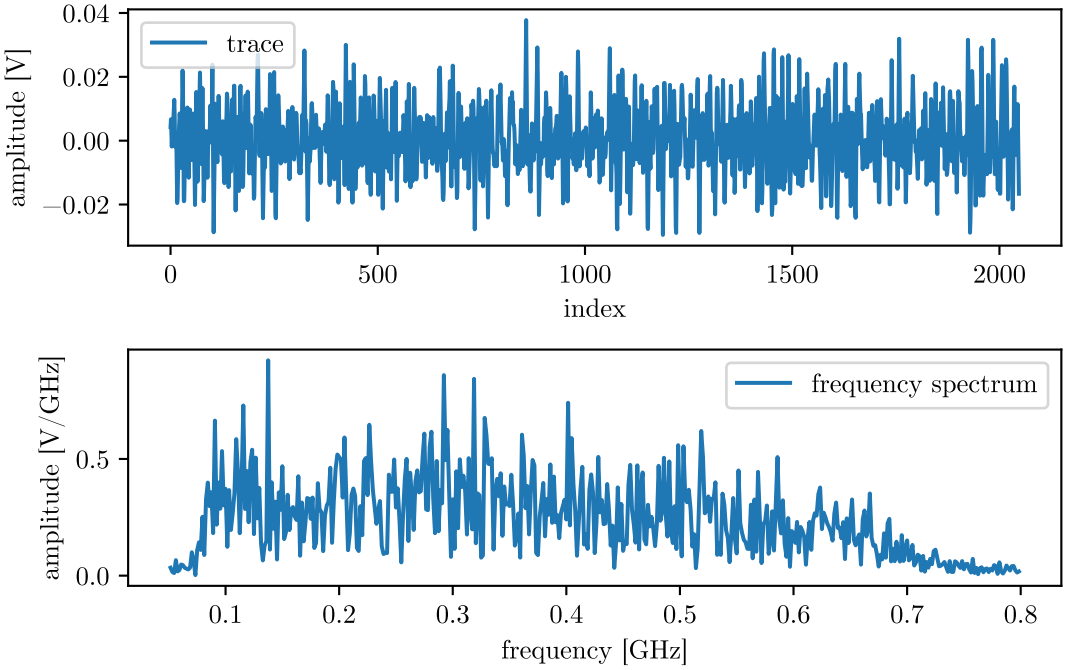

Figure 3: Example event measured in RNO-G.
Station Nr.: 11, Run Nr.: 1313, Event Nr.: 1, Channel Nr.: 13.
Top: The antenna voltage is shown over the index representing a whole trace with 2048 data points, over a duration of 640 ns.
Bottom: Corresponding frequency spectrum from 50 MHz to 800 MHz.
The signal is mostly noise.

transformation. When sampling data with 3.2 GHz it only makes sense to look at frequencies up to the Nyquist frequency of 1.6 GHz, otherwise effects like aliasing can produce artifacts in the data. Since signals only get amplified from $\sim$ 80 MHz to $\sim$ 750 MHz, this is the bandwith of interest, that will be focused on.

2.4 Backgrounds

Depending on the model [3] the expected number of interacting neutrinos in the fiducial volume of RNO-G (35 station layout) is $0.1 - 1$ neutrinos per year. The average trigger−rate in one station is $\sim$(0.5 Hz). The average trigger−rate for single runs varies from run to run, normally it is in the region from 0.2 Hz to 1.25 Hz. The maximal possible trigger−rate is $\sim$ 30 Hz, due to a dead time in the station after each triggered event [3]. Force−triggers are triggered with 0.1 Hz, so there is $\sim$ 1 background/noise event every 2.5 s. Therefore one of the main challenges for RNO-G is effective background discrimination. A lot of backgrounds were already observed and identified. The following is an overview of what has been found so far [13].

Thermal Noise: Thermal noise is a constant background. The movement of electrons in the antennas is statistical and therefore is the measured voltage. Just by chance

it will happen from time to time that the voltage in multiple antennas exceeds the threshold and a trigger criterion is met, without an actual event taking place. The event in Figure 3 is assumed to be such a noise event.

Solar Panels: Battery charging from solar panels was identified to cause background events in early stations during daytime. The hardware has been changed for stations deployed in 2022 or later.

Wind Turbines: Wind turbines were tested in stations 11 and 12 as a potential power source during winter. However they have been found to contribute to background events.

LoRaWAN: The LoRaWAN system is used to transfer station data to Summit Station where it gets stored on hard drives. It has been found to emit impulsive signals that can be seen by the detector. Changes in the hardware were made to prevent this from happening in stations from 2022 onwards.

CW: Continuous wave (CW) events (more in section 4.1) from different origins were found. CW signals are human made narrow band signals, used for data transfer. Including air traffic (125 MHz, 152 MHz), walkie−talkies (136 MHZ, 152 MHz), weather−balloon (402 MHz) and additional lines at 200 MHz and 408 MHz of unknown origin.

Solar-Flares: Solar flares can be detected by RNO-G. Detailed information on Solar-Flare detection in RNO-G can be seen in [2].

Cosmic-ray air showers: Cosmic−ray air showers and cosmic−ray air shower induced muons are another source of radio background in RNO-G [14].

Wind: Wind was also identified to induce short pulse radio signals in the detector [13].

Another source that was identified to produce background events are aircrafts flying over RNO-G. Aircrafts feature a lot of technology used for navigation, communication and crash avoidance that sends radio frequency signals. Although it was possible to reconstruct the arrival direction of some signals detected in RNO-G, which matched with trajectories of airplanes passing the array, the conditions under which airplanes produce RF signals remain unknown. So does the actual noise source at the airplane. Potential scenarios are discussed in section 3.3.

2.5 Flight tracker

Airplane detection at RNO-G is done with the so called flight tracker. RNO-G makes use of the Automatic Dependent Surveillance – Broadcast (ADS-B) system. It is a non-centralized surveillance system for airplanes, designed for regions without ground based radar surveillance. Airplanes track their own position and speed via GPS. Every modern airplane is obligated to broadcast these information via the 1090 MHz band. At the top of summit station there is a commercial antenna tuned for ADS-B data. It can receive flight data in a distance up to 400 km. The received messages get digitized

ADS-B Message Key Information

Bit	No. bits	Abbreviation	Information
1–5	5	DF	Downlink Format
6–8	3	CA	Transponder capability
9–32	24	ICAO	ICAO aircraft address
33–88	56	ME	Message, extended squitter
(33–37)	(5)	(TC)	Type code
89–112	24	PI	Parity/Interrogator ID

Table 1: Length and information contained in different ADS-B message parts.

by a raspberry pi. An ADS-B message is 112 bits long and consists of 5 main parts [16], those can be seen in Table 1.

Downlink Format:
The first 5 bits contain the Downlink Format (DF) information. Mode S transponder based civil aircrafts use Downlink Format 17. Non-Transponder-based ADS-B Transmitting Subsystems and TIS-B (Traffic information service – broadcast) Transmitting equipment use Downlink Format 18. An ADS-B/TIS-B Subsystem reiceiving messages with Downlink Format 18, instead of 17, knows that the message comes from equipment that cannot be interrogated [16].

Transponder Capability:
The second part of the message is the Transponder Capability, more information can be obtained in [16].

ICAO:
Each aircraft can be identified by its unique Mode S transponder code assigned according to ICAO (International Civil Aviation Organization) regulations [7]. The Mode S transponder code is also refered to as ICAO code or hexcode.

Type Code:
The Type Code (TC) specifies which information is given in the actual ADS-B message. The aircraft's flightnumber is sent in an identification message. Position and velocity information is sent separately in position, velocity messages. This is why it is possible to lose flightnumber information of an aircraft but still be able to see its position. Especially because the position messages get send 10 times as often as the identification messages as can be seen in Table 2.

From all messages received for a plane, every 5 seconds the following values are calculated [12]:

Frequency of ADS-B message emission

Messages	TC	Ground (still)	Ground (moving)	Airborne
Aircraft identification	1–4	0.1 Hz	0.2 Hz	0.2 Hz
Surface position	5–8	0.2 Hz	2 Hz	-
Airborne position	9–18, 20–22	-	-	2 Hz
Airborne velocity	19	-	-	2 Hz
Aircraft status	28	0.2 Hz	1.25 Hz	-
Target states and status	29	-	-	0.8 Hz
Operational status	31	0.2 Hz	0.4 Hz	1.25 Hz

Table 2: Different types of ADS-B messages and how frequently they get sent.

Flightnumber: the flightnumber / callsign

Lat, Lon: The aircraft position in latitude, longitude.

NUCp: The NUCp (navigational uncertainty category) reported for the position.

Seen_pos: How long ago (in seconds before "now") the position was last updated.

Altitude: The aircraft's altitude in feet, or "ground" if the plane is on ground.

Vert_rate: Vertical rate in feet/minute.

Track: True track over ground in degrees (0-359).

Speed: Reported speed in kt. This is usually speed over ground, but might be indicated airspeed (IAS).

Messages: Total number of Mode S messages received from this aircraft.

Seen: How long ago (in seconds before "now") a message was last received from this aircraft.

RSSI: Recent average RSSI (signal power), in Dezibel relative to Full Scale (dBFS); This will always be negative.

This information gets stored in a daily sqlite file, which can be downloaded from [8]. In the current software implementation NUCp, seen_pos and messages are not contained in the downloadable data [9]. NUCp is used to quantify the uncertainties on the planes GPS position. This precision would anyways most likely have been dominated by the timing uncertainty between aircraft and flight tracker time.
The flight tracker got deployed in 2021 and is taking data since 2021-06-16. Till 2024-06-17 it had the downtimes seen in Table 3, meaning no flight data was stored during this durations.

Flight tracker downtimes

2021-06-22	2021-07-11	2021-07-20	2021-08-07	2023-06-19	2023-08-12	Total
5	5	6	8	2	33	59 / 1097

Table 3: Dates of last reception of flight tracker data at RNO-G followed by a downtime of x days. In total, 1097 days of runtime from 2022-06-16 till 2024-06-17 were investigated.

3 Airplanes at RNO-G

This section will provide some basic statistical information about planes flying over RNO-G. Skiers and commercial airliners and their abundance are discussed separately. Plane trajectories are shown and observations about typical behaviour are discussed. Finally potential noise sources at airplanes are discussed.

For the analysis the period from 2021-06-16 till 2024-06-17 was chosen. During this time there was a total of 7800 planes passing RNO-G at a distance of 50km. This is defined as at least one datapoint in the flight tracker data beeing closer than 50 km to RNO-G (distance calculated in 3D). This makes an average of 7 planes per day, although the actual number varies greatly from day to day and also over the years. Among those were 102 skiers, as discussed below. Then there are commercial airline jet planes, they usually pass RNO-G at a height of around 10 km in relatively straight lines. Airliners will be discussed in section 3.2. A non negligible percentage of 6.5 % of the total time at least one plane was closer than 50 km to the array.

3.1 Skiers

Skiers are propeller airplanes, of the type Lockheed LC-130 Hercules, equipped with skies in order to be able to land on snow. Their purpose is to deliver supplies and staff to Summit Station. They fly at around 3 km height, often times circling Summit Station before landing at the skiway. Circling around the runway is a typical behaviour when landing a plane on sight. The so called downwind leg is a procedure where the pilot flies parallel to the runway but in opposite direction, preparing the descend. A skier can be identified by it's flightnumber, mostly the first 5 characters are "SKIER" followed by a number from 10-99. But there are some exceptions. All observed flightnumbers from skiers are listed in Table 4. Skiers were flying with 84 unique flightnumbers but there was only a total of 12 unique aircrafts. Their hexcodes (ICAO aircraft adresses) can be seen in Table 5.
The number of skiers can be seen in Figure 4, it was only plotted for 2 radii (2 km, 50 km), as there is no great variation for different radii. Most of the skiers that were seen proceeded to land at RNO-G. Due to weather conditions sometimes it is not possible to land. There is no skier traffic during winter time as the conditions in Greenland are to harsh during winter.
In Figure 5 and Figure 6 typical trajectories for Skiers can be seen. Skiers often times circle summit station at least once before landing. In the detector data there often are short intervals with a high number of cw (section 4.1) events during this period. One example is shown in Figure 20. However this can be observed for most of the skiers. The cw events are mostly on known walky-talkie frequencies like 151.6 MHz. Most likely this is due to the communication of the skier and summit station.

3.2 Airliners

One can see that the number of planes passing RNO-G per month varies heavily over time. There are not many flights in 2021, this might be due to airplane traffic still being restricted because of the corona virus pandemic. From start to middle of 2022 the numbers go up quite rapidly. In February 2022 Russia invaded Ukraine, therefore

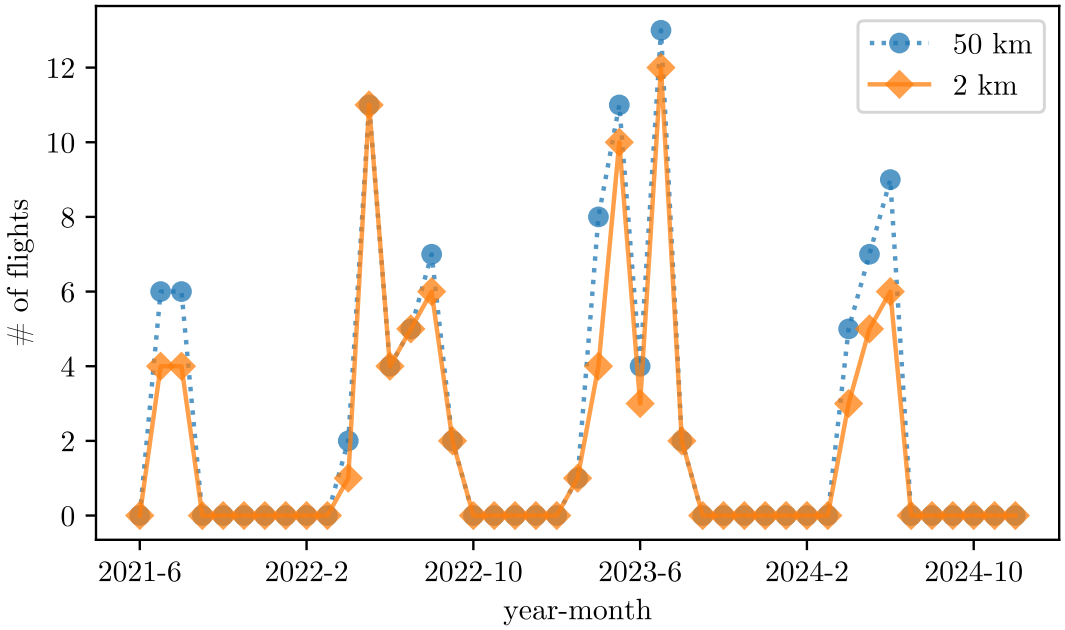

Figure 4: The number of Skiers at RNO-G per year−month from 2021-06 till 2024-07 for different radii (3D).

Flightnumbers of skiers at RNO-G

SKIERn	CFKBX	RCH10	CGOOU	CGEAJ	SKI043
94	2	2	2	1	1

Table 4: Flighnumbers of skiers at RNO-G and their occurance from 2021-06-16 to 2024-06-17. SKIERn were seen with different flightnumbers were n ϵ [10, 99].

airspace above Russia and Ukraine was blocked for civil aircrafts. Alternative routes e.g. over Greenland should see increased usage. At the end of 2022 the numbers of flights go down to a baseline of $\sim$ 200 flights per month in a 50 km radius. There is another peak in July 2023 followed by a sharp decline in August 2023. As can be seen in Table 3, from 2022-08-12 on, the flight tracker had a downtime of 33 days, therefore the real number of flights in august remains unknown. Afterwards the numbers alternate roughly around a baseline of $\sim$ 200 flights per month.
The first 3 letters of the flightnumber indicate the airline the plane belongs to. The top 10 airlines (r = 50 km) are listed in Table 6.

When looking at the top 4 airlines (combined with N/A flightnumbers) over different radii, which can be seen in Figure 8, one sees different behaviour. For the airlines ANA, JAL there is a rapid increase from basically no flights up to a constant number independent of the radius. For KLM and DLH the number of flights increases in 3 steps. The number of flights where the flightnumber is unknown (N/A) increases quite heavily at around 80 km radius and then seems to saturate for large radii. In order to understand what is happening one has to take a closer look at the trajectories of those

ICAO adresses of skiers at RNO-G

adfdee	ae060f	ae0610	adfdb4	ae0635	ae060e
18	12	11	11	9	7

adfdb5	ae0607	ae0608	c06b21	c04f42	c01a9a
6	5	2	1	1	1

Table 5: ICAO aircraft addresses of skiers at RNO-G and their occurrence from 2021-06-16 to 2024-06-17.

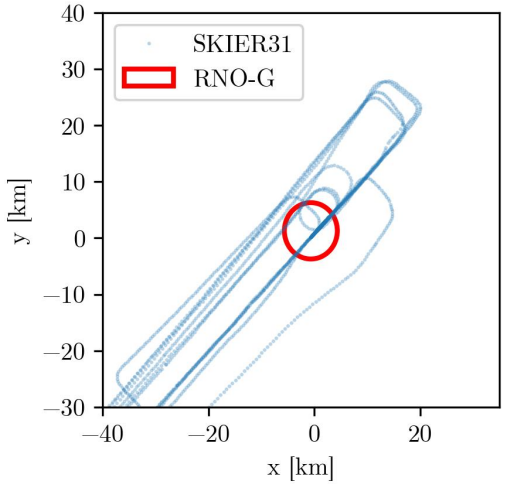

Figure 5: Trajectories for all flights of SKIER31. The RNO-G array is marked in red.

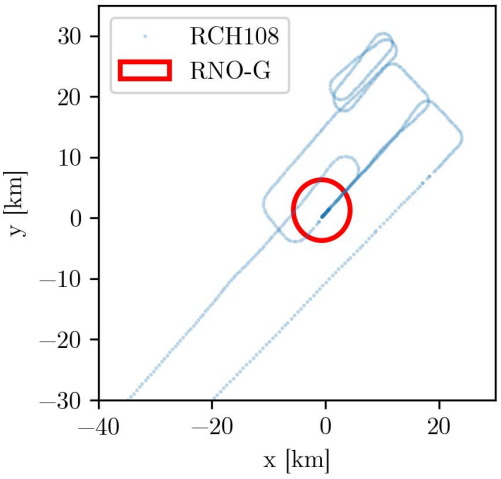

Figure 6: Trajectory for one flight of Skier RCH108. The RNO-G array is marked in red.

airlines. This will be discussed in the following.

KLM

Flights of KLM, as seen in Figure 9, mainly pass RNO-G in the same sectors. That is why in Figure 8 one can see the number of flights go up in 4 steps. The first one being at around 40 km where the sector north−west of RNO-G becomes visible. The second sector is at around 80 km south−west of RNO-G. The third at around 125 km, also north−west. Finally the 4th sector can be seen at a distance of $\sim$ 175 km south−west of RNO-G. There are a few flights outside of these sectors, but most of them follow the same routes.

DLH

The same behaviour as for KLM can be seen for DLH (Figure 10). Planes do mainly fly through the exact same sectors despite being from a completely different airline.

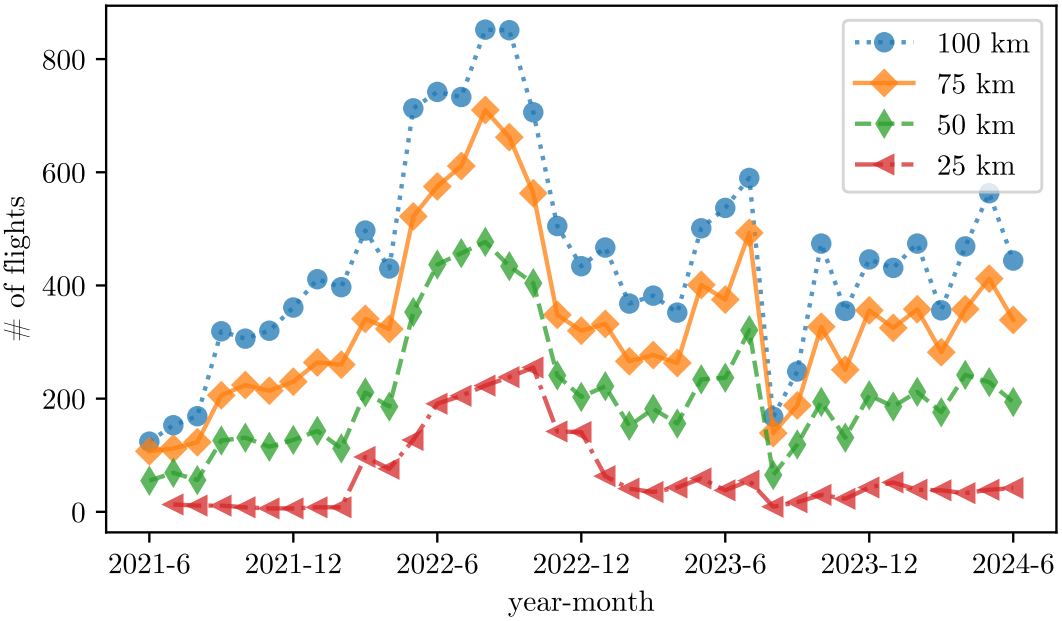

Figure 7: The number of flights over RNO-G per year-month from 2021-06 till 2024-07 plotted for different radii (3D).

Top 10 airlines seen at RNO-G (r = 50 km)

DLH	ANA	JAL	KLM	THY	SAS	AFR	DAL	CFG	QTR
1228	762	724	705	548	457	441	405	268	249

Table 6: Top 10 airlines seen at RNO-G (r = 50km) ordered by their occurrence.

JAL & ANA

When looking at the two japanese airlines Japan Airlines (JAL) and All Nippon Airlines (ANA) one observes really strange behaviour (Figure 12, Figure 11). All aircrafts fly above (north of) a line that passes directly through RNO-G from north−west to south−east. One does even see planes flying sharp corners when hitting the line from another angle. This behaviour can also be observed when looking at single flights. At the moment it is unclear wether this is a bug in either the flight tracker software or in the code that was written for this thesis or if this is the reality. This behaviour can only be observed for the two japanese airlines. Planes of other airlines also often take the exact same routes, but it seems strange that RNO-G by coincidence was build exactly where every japenese airliner tries to cross Greenland.
An exact depiction of how the stations are contained in the red circle and a screenshot of the flight trajectory of JAL43 (Tokio Int'l (Haneda) − London Heathrow, 2024-09-06) as seen by [10] are included in the appendix.

N/A

Datapoints with flightnumber N/A can be seen in Figure 13. When the flightnumber is N/A this usually means that position messages get received by the FlightTracker

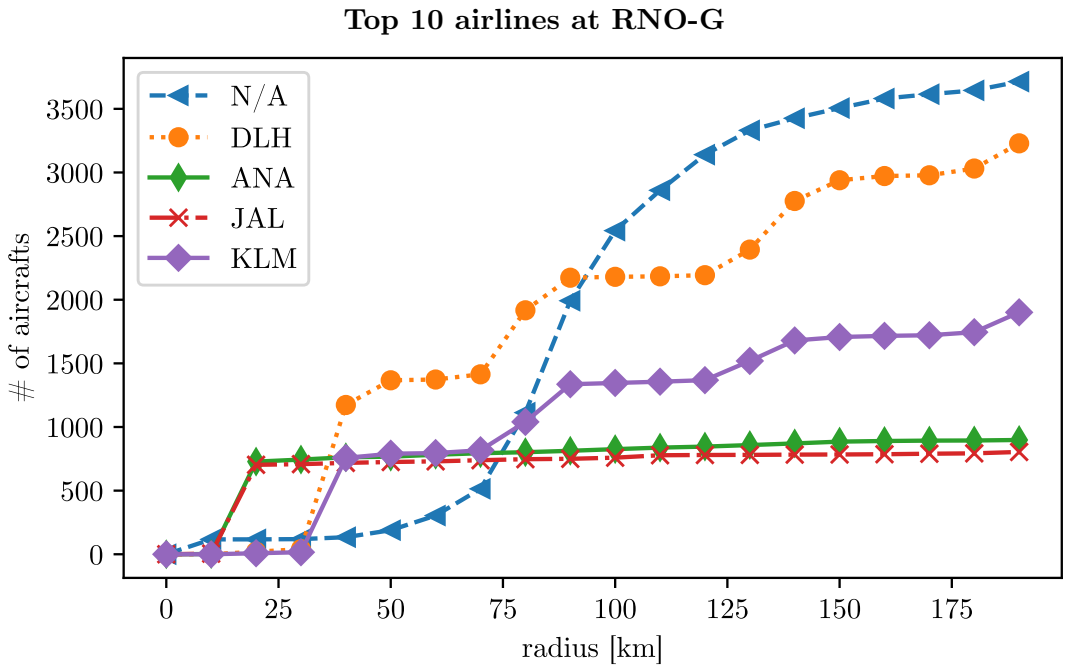

Figure 8: The number of flights ar RNO-G per airline for different radii (3D).

but not identification messages. This can happen from time to time, especially because the position messages get sent 10 times more often than the identification messages. If one looks for increasingly big radii the number of N/A flights go up quite rapidly, but this usually does not mean that there are whole trajectories of planes with unresolved flightnumber. These are just single (or some) datapoints in the trajectory of a plane with resolved name. If the radius is big enough one can find such a datapoint in almost every plane's trajectory, therefore the number of N/A flights saturates eventually.
Interestingly in Figure 13 the FlightTracker seems to lose connection to the planes more often in the east of RNO-G. One explanation could be that there are more planes travelling from west to east and the ADS-B information gets broadcasted to the front, after all this is a collision avoidance system. But in reality about 3/5 of all flights go east−west and only 2/5 go west−east. Also when looking at single flights that lose connection one can see a lot of them travelling east−west. Therefore it is more plausible that this behaviour is due to certain antenna positioning.
The N/A datapoints that can be seen exactly at RNO-G's position stem from skiers that landed at the detector. This was found by comparing the hexcodes from N/A flights and skiers.

3.3 Possible noise sources in airplanes

As seen in section 3.2 there is a lot of air traffic going on at RNO-G. This section shows the potential problems arising from planes flying over RNO-G. There are many different types of airplanes passing by RNO-G, but they should have most of their functionality in common. In order to show potential noise sources the antennas and probes of an Airbus A320 Aircraft are discussed. The following information and figures are taken from [11].

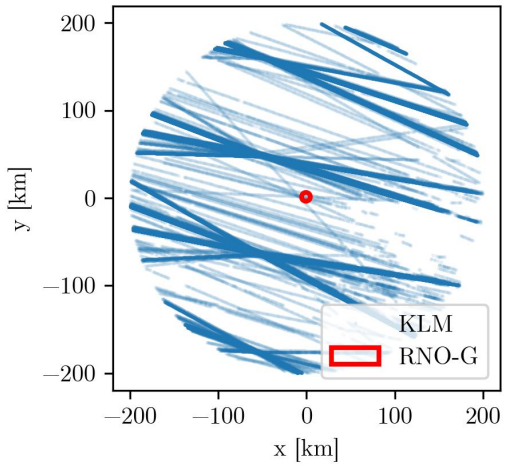

Figure 9: Trajectories for all flights of Royal Dutch Airlines (KLM) in a radius of 200 km. The RNO-G array is marked in red.

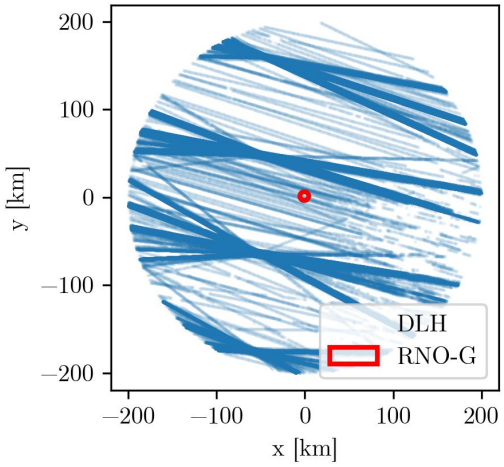

Figure 10: Trajectories for all flights of Deutsche Lufthansa (DLH) in a radius of 200 km. The RNO-G array is marked in red.

WEATHER RADAR – The WXR the weather radar is used to detect and track weather conditions, particularly precipitation like rain, snow and hail. It sends out radar signals and determines weather condition by the strength of reflected signal. In theory the frequency of those signals should by above 2 GHz and therefore outside the range, that is detected by RNO-G.

VHF The Very High Frequency (VHF) antenna is used for communication in the VHF frequency range (30 MHz - 300 MHz). This falls into the region of interest of RNO-G. As these signals should be cw it is rather easy to filter those events in the detector data (section 4.1).

HF The High Frequency (HF) antenna is used for communication in the HF frequency range (3 MHz - 30 MHz). It is used for long range communication. The frequency range should not be detected by RNO-G. But otherwise the procedure of filtering those signals out is the same as for VHF.

TCAS The Traffic Collision Avoidance System (TCAS) works similarly to ADS-B. Messages get sent/received at 1030 MHz and 1090 MHz. So there should not be interference with RNO-G.

ELT The Emergency Locator Transmitter (ELT) antenna sends radio signals in the very high frequency (VHF) and ultra-high frequency (UHF) ranges in case of emergency. The ELT antenna transmits 406 MHz, 121.5 MHz, and 243 MHz signals. Although this is in the critical frequency range, those signals should not be sent unless there is a plane crash nearby.

RADIO ALTIMETER The RA antennas are usually on the bottom of the fuselage. Short pulse signals get sent to the ground, with their reflections the altitute of the airplane can get calculated. This is done to enhance GPS precision. Normally

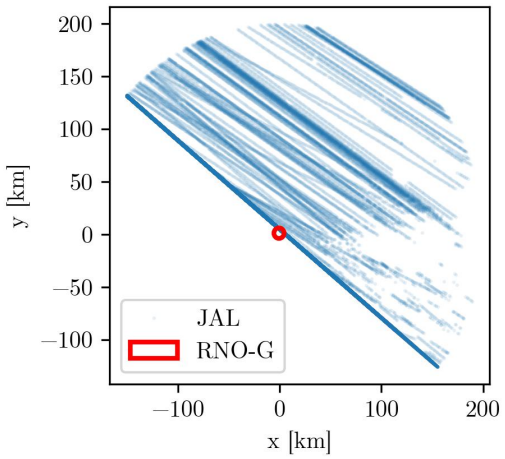

Figure 11: Trajectories for all flights of Japan Airlines (JAL) from 2022-06-16 to 2024-06-17 in a radius of 200 km. Data was recorded with the flight tracker at RNO-G. The RNO-G array is marked in red.

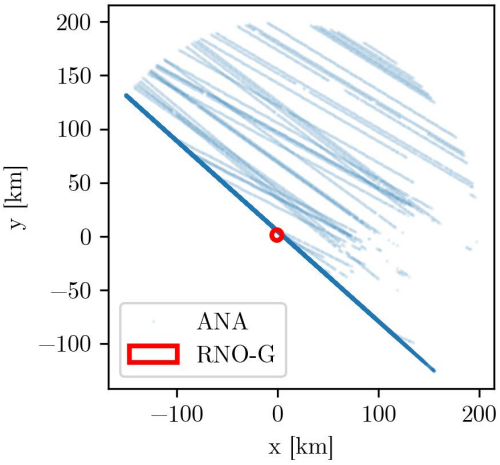

Figure 12: Trajectories for all flights of All Nippon Airways (ANA) from 2022-06-16 to 2024-06-17 in a radius of 200 km. Data was recorded with the flight tracker at RNO-G. The RNO-G array is marked in red.

it operates between 4.2 GHz and 4.4 GHz, this is outside the measured frequency spectrum in RNO-G.

DME The Distance Measuring Equipment (DME) antennas are used to determine the distance between the aircraft and a ground-based DME stations, by sending/receiving signals in the VHF range. It operates between 960 MHz and 1215 MHz, so technically there should not be interference with RNO-G

VOR The VHF Omnidirectional Range (VOR) antenna sends/receives RF signals in the frequency range of 108 MHz to 117.95 MHz.

Additionally to the equipment that sends signals the jet engines (propellers in Skiers) are another potential emitter of radio noise. At the moment it is not clear which equipment is responsible for radio interference, therefore everything has to be considered a potential background source.

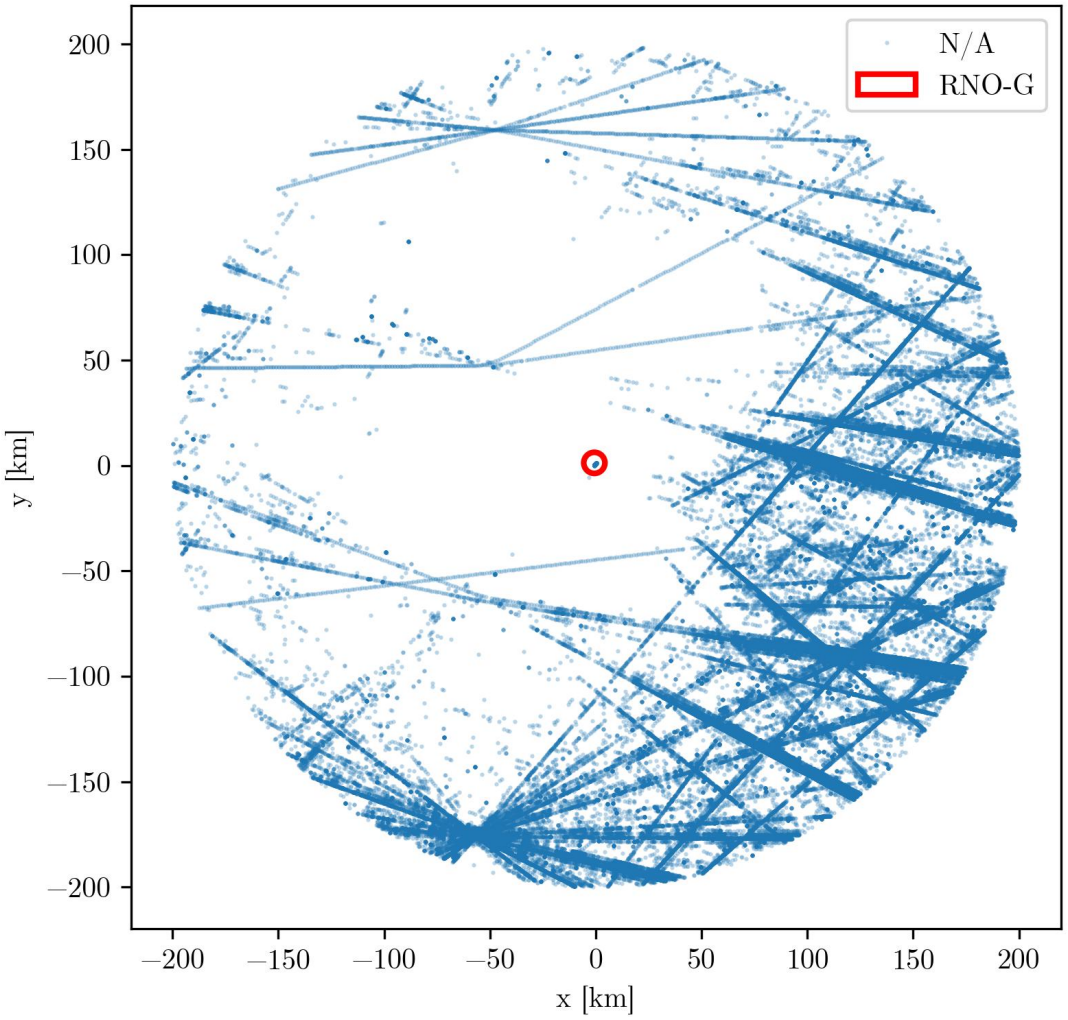

Figure 13: Datapoints with unresolved flightnumber from 2022-06-16 to 2024-06-17 in a radius of 200 km. Data was recorded with the flight tracker at RNO-G. The RNO-G array is marked in red.

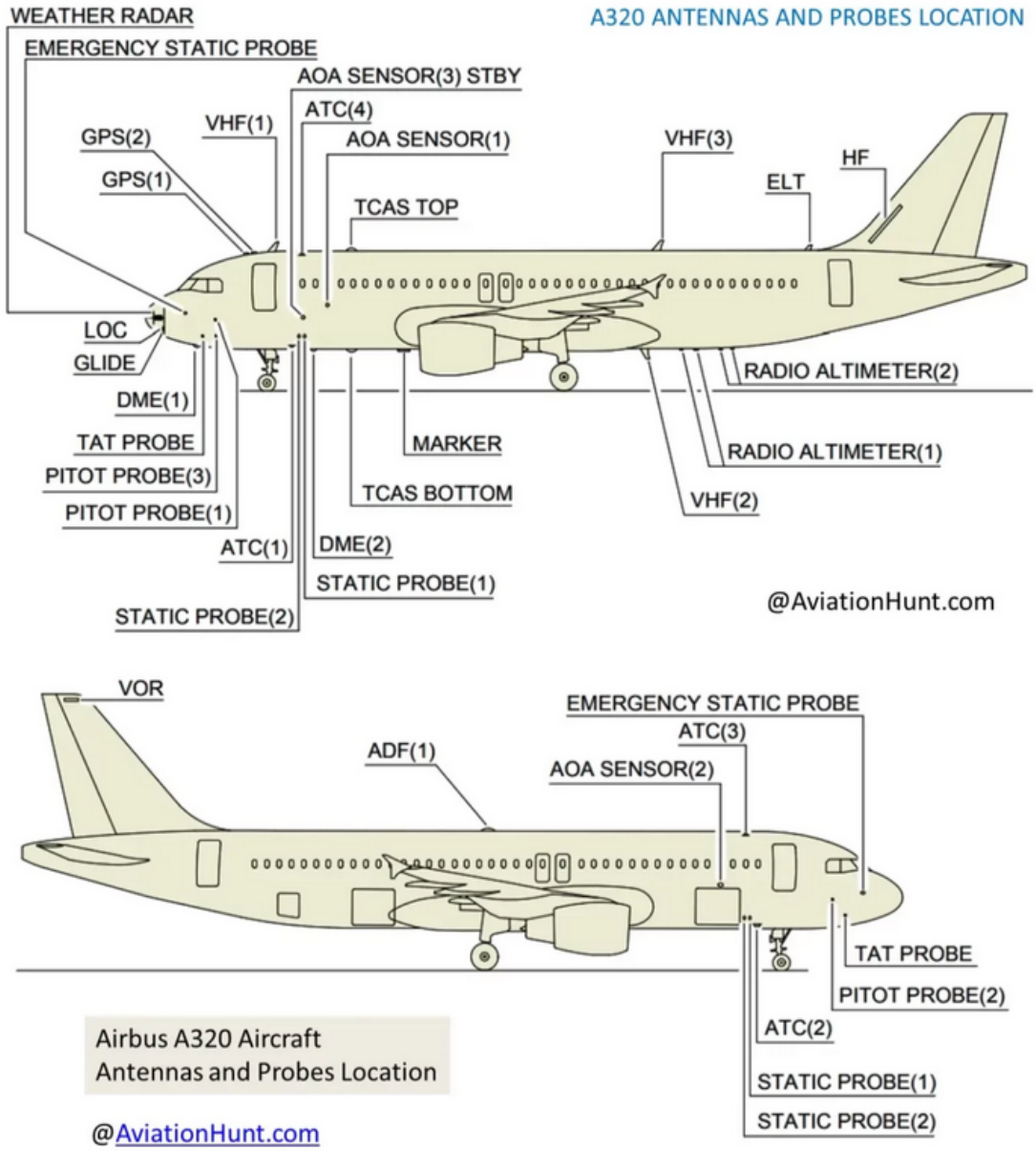

Figure 14: Antennas and Probes of an Airbus A320 are depicted, taken from [11]

4 Methods

In this sections the methods that were used in order to analyse airplane signals are discussed. 3 different scores are introduced. With their help signals can be analysed and their properties can be quantified on a single event basis.
Afterwards this is done for signals recorded by RNO-G, where their origin was traced back to stem from airplanes. Different behaviour of skiers and airliners are shown.

4.1 Scores

There is a broad range of signals that potentially get sent by airplanes. Communication is done on a single frequency, altitude measurements require short sharp pulses and engine noise can come in various shapes. Therefore one wants a way to identify and quantify different types of signals. In order to do so 3 scores that measure different signal properties are introduced.

Signal to Noise Ratio (SNR):
The Signal to Noise Ratio (SNR) measures the strength of the signal compared to the noise in the antenna. For every force trigger event in a given run the Root Mean Squared (RMS) per channel gets calculated. Let trace be the collection of data points given by the voltage measured in one channel over time. An element $x \in$ trace is a real number corresponding to the voltage at one given time. Let N be the total number of data points in trace. Then the RMS can be calculated as follows:

$$\text{RMS} = \sqrt{\frac{1}{N} \sum_{x \in \text{trace}} x^2}$$

Averaging the RMSs leaves an average RMS per station, channel and run. The Signal to Noise Ratio (SNR) for a given trace is its max absolute amplitude divided by the average RMS of it's run. An illustration is given in Figure 15. The RMS is strictly positive therefore it does not align with the average of the trace. The SNR gets calculated as follows:

$$\text{SNR} = \frac{\max_{x \in \text{trace}} |x|}{\text{RMS}}$$

L1 score:
The L1 score was used as a veto of narrow band signals in ARIANNA [6]. The implementation used here might differ from that in ARIANNA but when tuning the thresholds it serves the same purpose. The L1 score is a way to measure the periodicity of a trace. With the fourier transform one can extract the frequency spectrum of a signal. Periodic signals have sharp peaks in the frequency spectrum, where short impulsive signals consist of a broad range of frequencies. The L1 score measures how much of the signals power is contained in the frequency with the maximal amplitude. Let freq be the collection of data points given by the Fourier transform of the trace. An element $f \in$ freq is a real number corresponding to the absolute amplitude at a given frequency.

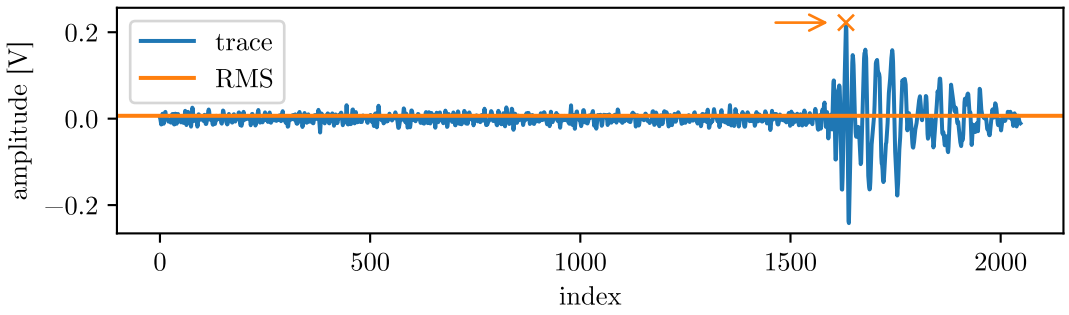

Figure 15: Example event measured by RNO-G.
Station Nr.: 11, Run Nr.: 1313, Event Nr.: 173, Channel Nr.: 13.
The antanna voltage is shown over the index, representing a whole trace with 2048 data points, over a duration of 640 ns. The highest amplitude is marked with a cross. The RMS = 6.34 e-3, maximal amplitude = 0.222 V, SNR = 35.1

Let N be the total number of data points in freq. The L_1 score gets calculated as follows:

$$L_1 = \frac{\max_{f \in \text{freq}} f^2}{\sum_{f \in \text{freq}} f^2}$$

A pure sine that consists of only 1 wave therefore would have a L1 score of 1. This score is particularly helpful when filtering for Continuous Wave (cw) signals, these are human made narrow band signals used for data transfer. Being able to identify cw is crucial for background discrimination, cw e.g. from walkie-talkies often comes with an increase in trigger rate.

Impulsivity:
The impulsivity score is used to quantify short, sharp pulses. It's calculation is more complex than for the other scores. First one has to calculate the Hilbert transform of a given discrete signal:

$$\mathcal{H}\{g[k]\} = h[k] * g[k]$$

where:

$$h[k] = \frac{1 - \cos \pi k}{\pi k}$$

It can be expressed as a complex series:

$$\mathcal{H}\{g[k]\} = \Psi[k] \exp\{iz[k]\}$$

where $\Psi[k] \geq |g[k]| \ \forall k$ is the hilbert envelope.
The hilbert envelope gets reordered starting with the index of highest amplitude at 0, then taking the neighboring indices in alternating order. This can be seen in Figure 17. Let reordered be the collection of data points given by reordering the trace. For the cumulative sum let $\text{reordered}_\text{i}$ be the sub collection of reordered containing only the first i elements. An element $r \in$ reordered is a real number corresponding to the absolute

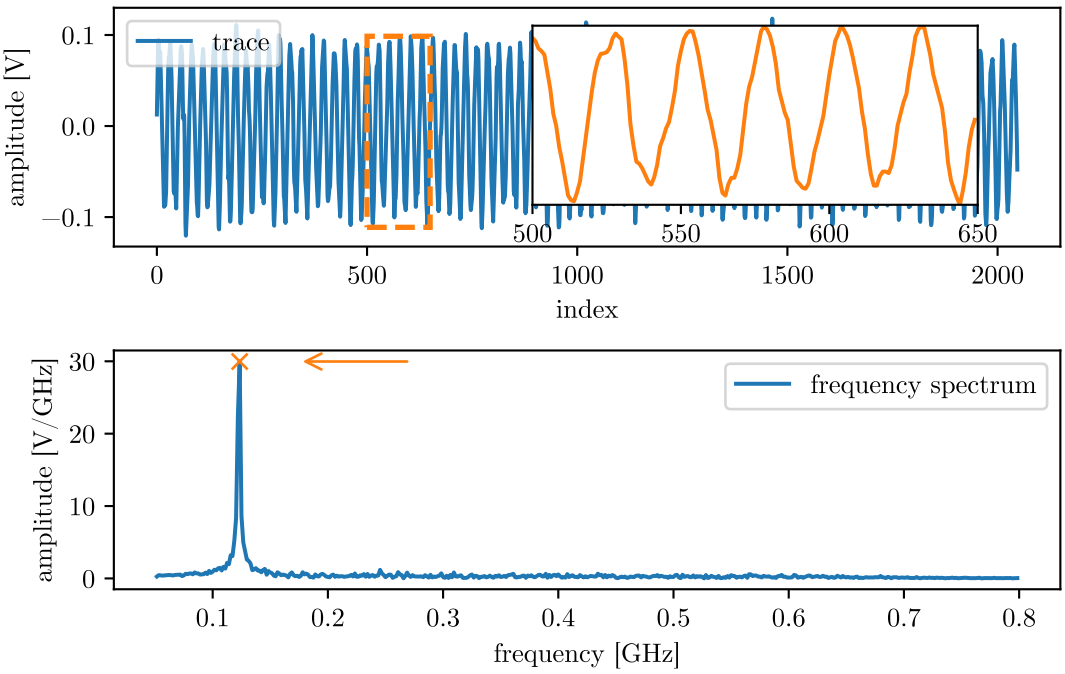

Figure 16: Example event measured in RNO-G.
Station Nr.: 11, Run Nr.: 1313, Event Nr.: 534, Channel Nr.: 13.
Top: The antenna voltage is shown over the index representing a whole trace with 2048 data points, over a duration of 640 ns. The signal is highly periodic, the sin wave is clearly visible in the 150 datapoints zoomed in (orange).
Bottom: The frequency spectrum of the signal is shown from 50 MHz to 800 MHz. A sharp peak is visible at a frequency of 123 MHz, L1 = 51.7.

amplitude of the hilbert envelope. Let N be the total number of data points in reordered. The impulsivity-curve gets calculated as follows:

$$\text{impulsivity\_curve}(i) = \frac{\sum_{r \in \text{reordered}_i} r}{\sum_{r \in \text{reordered}} r}$$

The average of the impulsivity_curve is what determines the impulsivity score of a signal. For shorter signals more of its total sum is contained in the region around the maximal amplitude, therefore the impulsivity_curve is steeper in the beginning and already closer to the total sum, resulting in a higher mean. The impulsivity is given by:

$$\text{impulsivity} = 2 \cdot \frac{1}{N} \cdot \sum_{i=1}^{N} \text{impulsivity\_curve}(i) - 1$$

The impulsivity_curve of a constant signal would lie exactly on the bisecting angle. If the calculated impulsivity would be negative it gets set to 0. Therefore the impulsivity score is contained in [0, 1[.

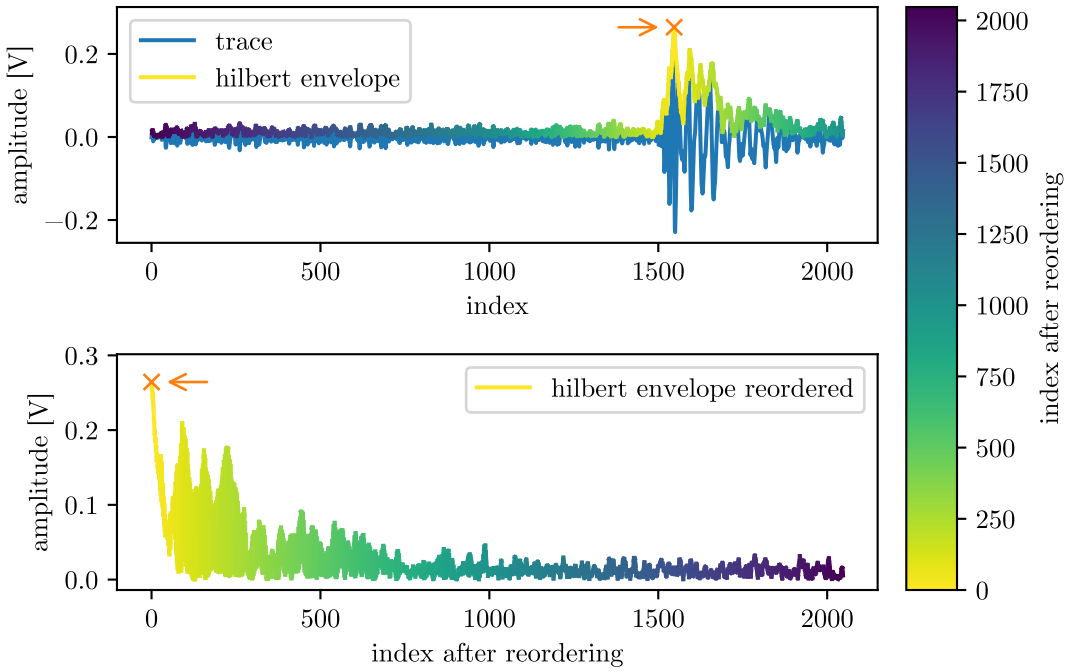

Figure 17: Example event measured in RNO-G.
Station Nr.: 11, Run Nr.: 1313, Event Nr.: 192, Channel Nr.: 13.
Top: The antenna voltage is shown over the index representing a whole trace with 2048 data points, over a duration of 640 ns. The hilbert envelope is plotted on top of the signal. The color indicates the index after reordering, due to the calculation of the impulsivity score. Reordering happens from the index with maximal amplitude on outwards.
Bottom: The 2048 data points after reordering.

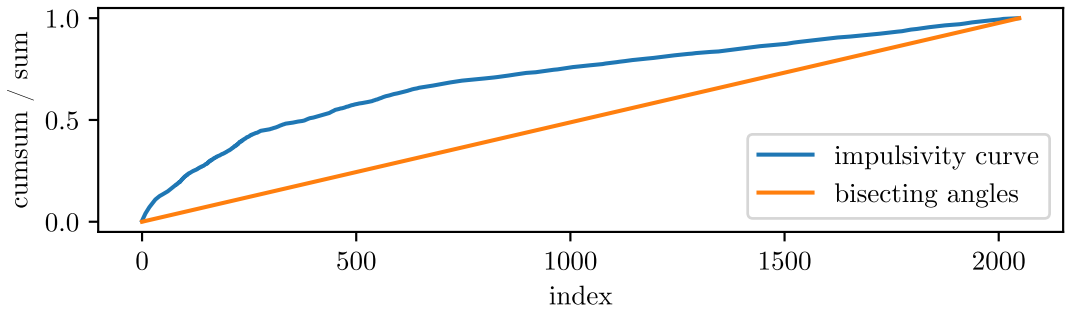

Figure 18: The impulsivity_curve for the event in Figure 17 is shown. The bisecting angles are plotted for comparison. The impulsivity_curve of a contant signal would lie on the bisecting angles. The cumulative sum divided by the total sum of the reordered hilbert curve is shown as a function of the index.

4.2 Airplane analysis

In this section aircrafts that are known to have emitted radio noise will be investigated. The flights were found by looking at coincident triggers in multiple stations. With triangulation it was possible to confirm that the signals stem from aircrafts, as there time and position fitted the FlightTracker data. For more details please have a look at [15].

The scores from section 4.1 will be plotted for station 11 as an example. Station 11 is not as noisy as some of the others. It got a hardware upgrade to get rid of LoRaWAN noise, also it does not have a windturbine which could induce noise. Besides that station 11 was chosen arbitrarily.

Skier31 2022-08-23:
Skier31 flew over RNO-G on 2022-08-23. It did a u−turn over the detector array before it proceeded to land. The planes trajectory, during the u−turn can be seen in Figure 19. The distance from plane to station 11, as well as the histogram of the trigger−rate and the Impulsivity, SNR and L1 score can be seen in Figure 20. The time interval with maximal signal brightness is marked in red. 3 clusters of events can be seen in the SNR score during that time, their mean frequency spectra are shown in Figure 21. Example events for every cluster of signals can be seen in the appendix.

The mean spectra for $10 < \text{SNR} < 50$ looks different than the other 2. It's main peak is at roughly 80 MHz. The other two mean spectra look quite similar. They have 3 main peaks around 100 MHz and roughly 190 MHz.

In all 23 traces contained in the cluster with $100 < \text{SNR}$ there is at least one false high peak like the one in Figure 38 marked with the arrow. This is an error introduced through an overflow glitch in the software. The very high peak increases the SNR, however there is no increase in impulsivity. This indicates that the two clusters above a SNR of 50 contain the same class of events.

Histogram:
The trigger rate increases when the plane enters a ∼10 km radius, it peaks for minimal distance of the plane.

L1 score
A slight increase of L1 score is visible for the ∼10km radius. Besides that, there are 3 "bursts", where L1 score goes up rapidly for a short period in time. The 3 bursts contain 2 frequencies as indicated in the figure. 151.6 MHz is used in walkie−talkies. Events with cw at 151 MHz can be seen for stations 11, 22 but not in stations 23, were 123 MHz is seen in all stations. Therefore 151 MHz could also be ground signals but not stem from the plane, 123 MHz on the other hand is most likely from the plane. After the u−turn the Skier proceeds to land at the skiway, which is not plotted in the figures. Therefore it could be that the communication seen in the data was some kind of request for permission to land.

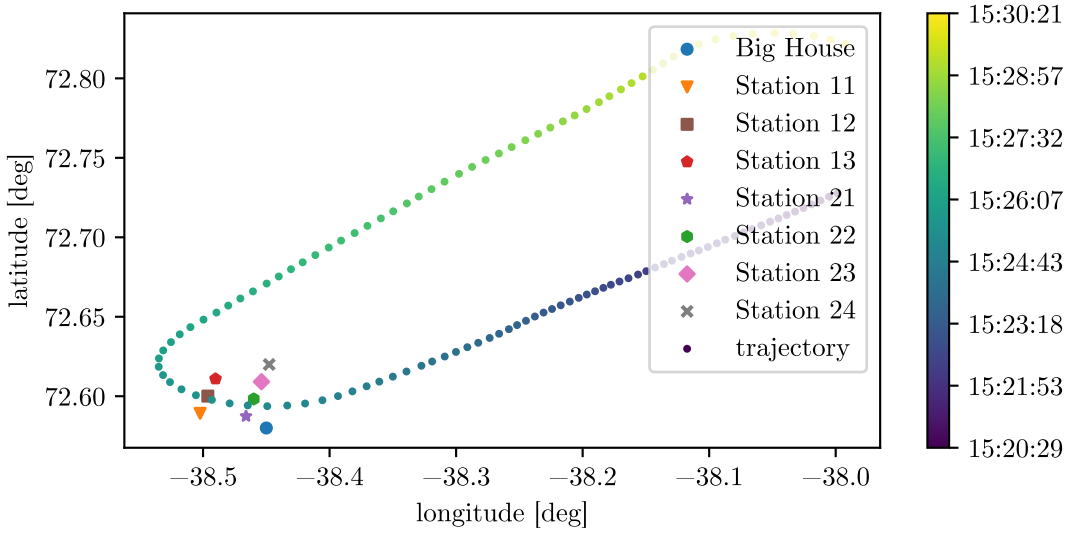

Figure 19: Skier31 on 2022-08-23 making a u-turn over RNO-G. Time is indicated by the colorbar. Each RNO-G station is depicted with another marker.

SNR

In the SNR when looking at the marked region in red, where brightness of the signal is maximal, one can see three clusters of events. In order to classify them one can calculate their mean frequency spectra. This is done in Figure 21.

Impulsivity

The impulsivity score rises for the same distance of the plane. Again there are 2 categories of events. In the arch there are some gaps. If there is some cw present in the trace, even if the event is dominantly impulsive, the impulsivity score gets pulled down, because the surrounding neighborhood of the high pulse does not get compared to noise, but rather to a weak cw signal, that has higher amplitude.

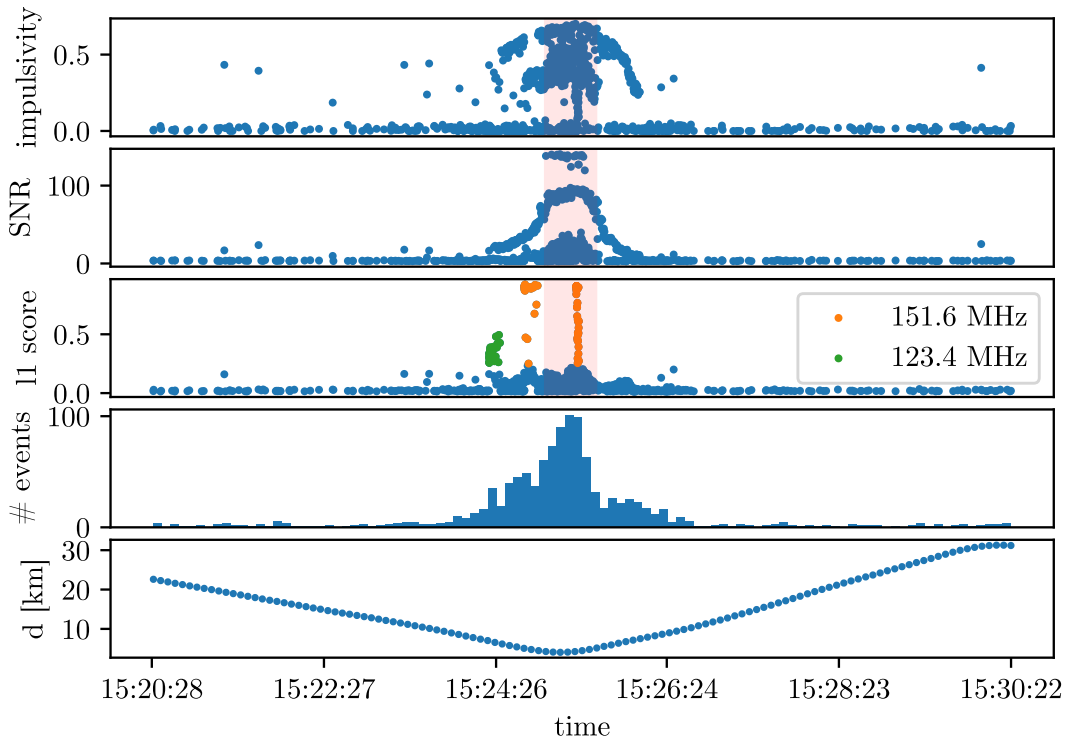

Figure 20: Scores for Skier31 on 2022-08-23 flying over RNO-G. Scores calculated for each radiant trigger event are shown for station 11 channel 13 (upward facing LPDA). The first 3 axes display impulsivity, SNR and L1 score over time. The fourth is a histogram of the trigger time. The fifth displays the 3D-distance of the plane to station 11. Signal brightness and trigger−rate correlates with the planes distance. There are 3 bursts of cw events. The time interval with maximal signal brightness is marked in red. In this interval there are three clusters seen in the SNR.

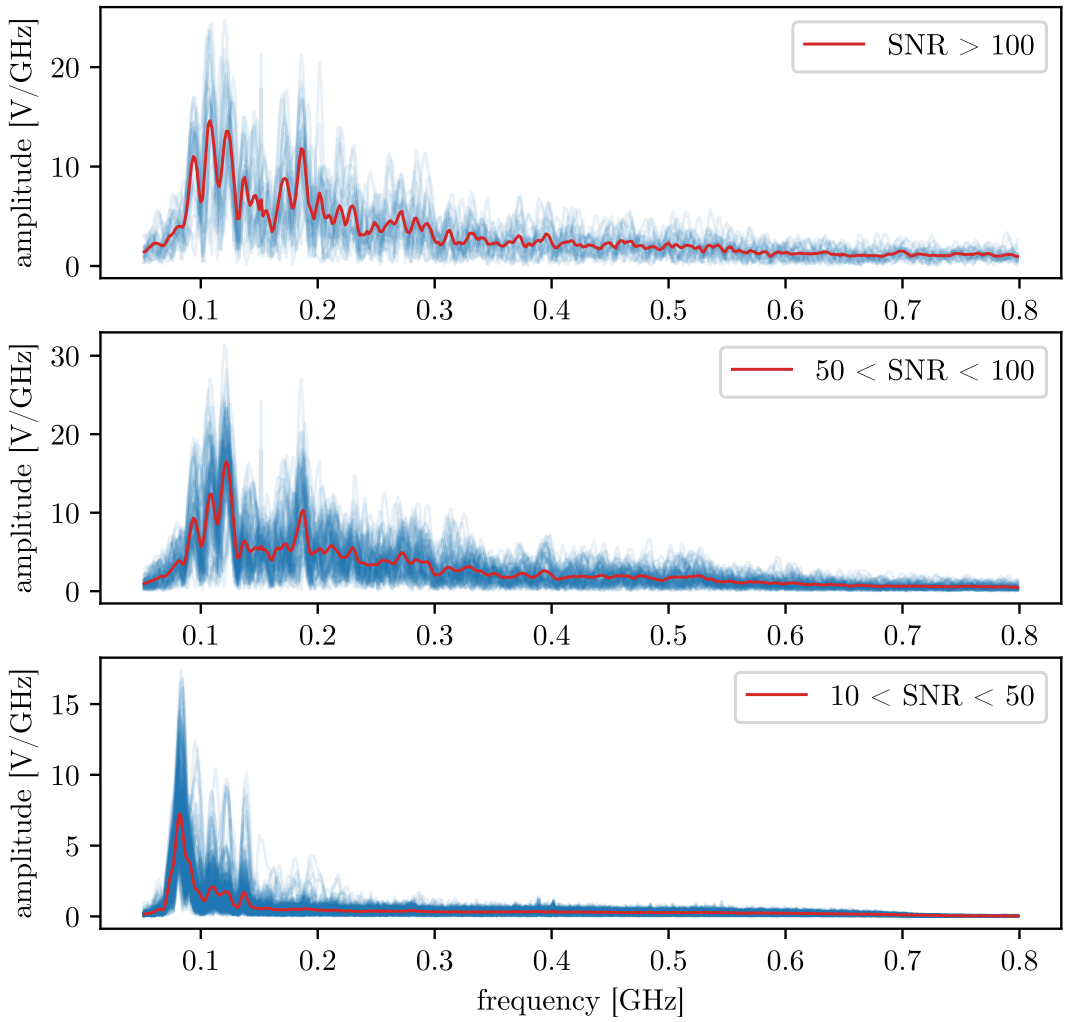

Figure 21: The mean spectrum for the three clusters of events seen in SNR (marked region), in Figure 20, is plotted in red. In blue the actual spectra of every single event were plotted with a low alpha value.

JAL43 2022-08-17:
Flight JAL43 flew over RNO-G on 2022-08-17 in a relatively straight line. After it passed the array a cluster of signals could be detected. The region is marked with red. Before it reached the array there was a short burst of cw measured by the detector. The trajectory of JAL43 can be seen in Figure 22. SNR, Impulsivity and L1 score, as well as a histogram of the trigger−rate and the distance from plane to station 11 can be seen in Figure 23. The average frequency spectrum of the events contained in the red region can be seen in Figure 24.

Histogram:
For the JAL flight there is no increase of trigger−rate that correlates nicely with the distance from plane to detector. We rather see a short cw burst before the plane flies over RNO-G and a wider cluster of events after the plane is directly above RNO-G. The plane is flying at around 10km height, so at 10 km distance (3D) the plane is exactly above RNO-G .

L1 score:
As already mentioned the L1 score is rather high for the short burst, but there is no increase in L1 score for the bigger cluster of events. So the short burst contains cw and the events in the cluster are of some other type.

SNR & **Impulsivity**:
In the big cluster all events have high SNR and are also impulsive. Besides that there is no rise in SNR or Impulsivity that correlates with the planes distance.

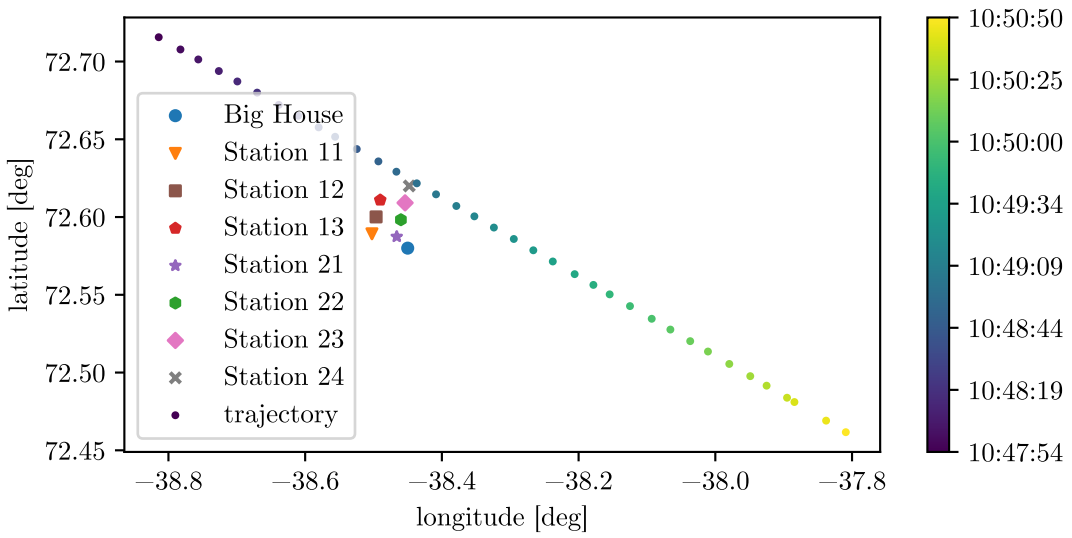

Figure 22: Flight JAL43 flying over RNO-G on 2022-08-17 in a straight line. The datapoints are taken from the FlightTracker. Time is indicated by the colorbar.

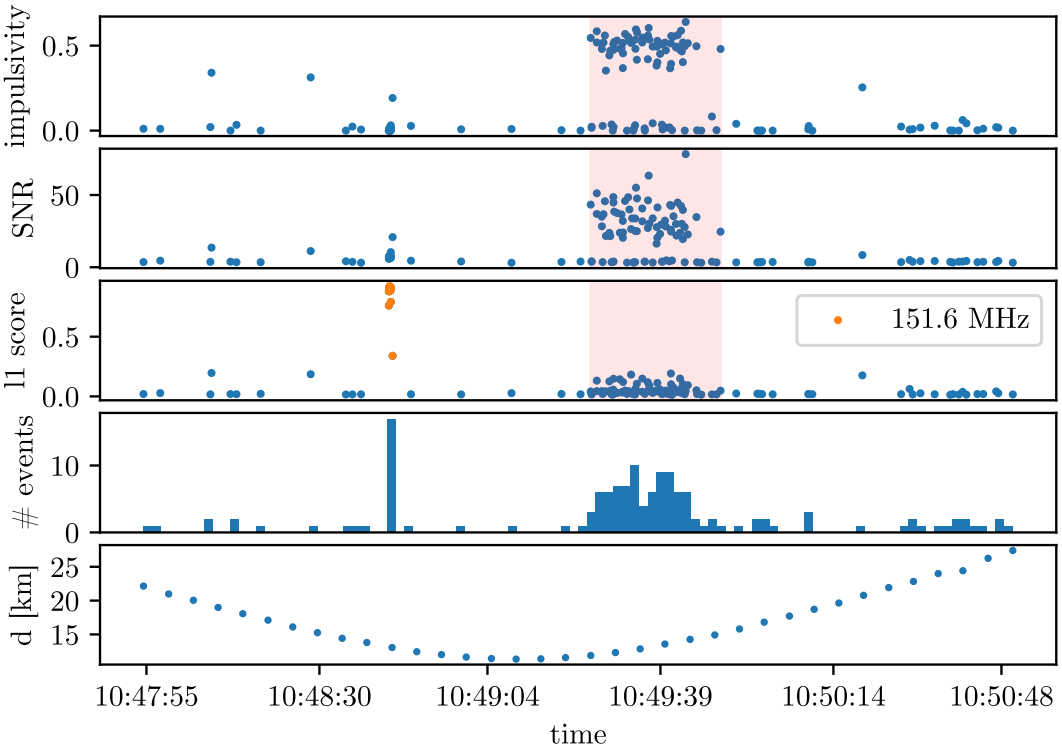

Figure 23: Scores for JAL43 on 2022-08-17. The scores are calculated for every radiant trigger event for station 11 channel 13 (upward facing LPDA) during the flight. The first 3 axes display impulsivity, SNR and L1 score over time. The fourth is a histogram of the trigger time. The fifth displays the 3D-distance of the plane to station 11. The region with high impulsivity is marked in red. There is no correlation between the planes distance and the events seen in the detector. Before the plane was above RNO-G a short burst of cw can be seen. After the plane passed RNO-G it sent RF signals in a short time interval $\sim$ 30 sec.

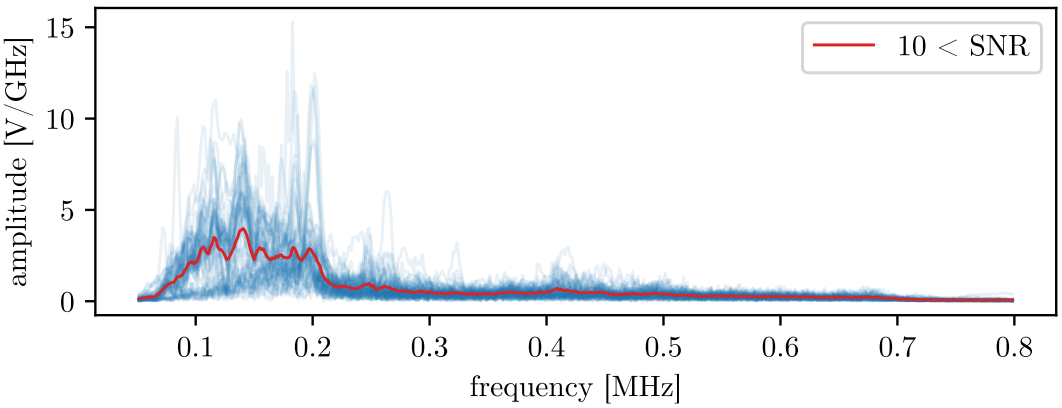

Figure 24: Mean frequency spectrum for the clusters of events seen in SNR (marked region) in Figure 23. Every spectrum was plotted in blue with a low alpha value. The mean spectrum is was plotted on top in red.

CPA085 2023-05-07:
Flight CPA085 passed RNO-G on 2023-05-07 in a straight line. When it was right above RNO-G a it emitted RF signals that were detected by RNO-G. The SNR, Impulsivity and L1 score as well as a histogram of the trigger−rate as well as the distance from plane to station 11 are shown in Figure 26. Two types of signals could be seen. They are contained in the region marked in red. The mean frequency spectra of these events are shown in Figure 41. Example events of each type can be seen in the appendix.

Histogram:
Similar to JAL43 there is no increase in trigger rate that correlates nicely with the distance from the plane to station 11. There is no visible increase in trigger rate at all.

L1 score:
The highest L1 score is around 0.2, that is not considered to be cw.

SNR & **Impulsivity**:
There are 3 small clusters with high impulsivity and SNR, consisting of 2, 3 and 5 events. When looking at the mean spectra one sees that there are two types of events. The first one with the main peak in the frequency spectrum at around 80 MHz, the second one with the main peak at around 175 MHz. In the following they will be classified as freq_max < 0.1 [GHz] and freq_max > 0.1 [GHz]. The events > 0.1 [GHz] are shorter, more impulsive as the impulsivity score already suggests. They peak and then swing out fast. For events < 0.1 [GHz] it takes longer to swing out, during that period there is a higher cw component in the trace. Therefore those events have the higher L1 score.

Summary:
From the 3 flights discussed one can already tell that there is a broad range of different signals emitted by planes. Lots of them are impulsive with the potential to interfere with neutrino analysis. Skiers seem to be quite noisy, due to the way they are constructed, but also because they come much nearer to the array. On the one hand this introduces more noise, but also makes it easier to spot a nearby skier, potentially from detector data only. Commercial airliners are more difficult to spot because there seems to be no correlation between the distance of planes and the magnitude of signals emitted. Rather 'spontaneous' emissions at random locations can be observed.

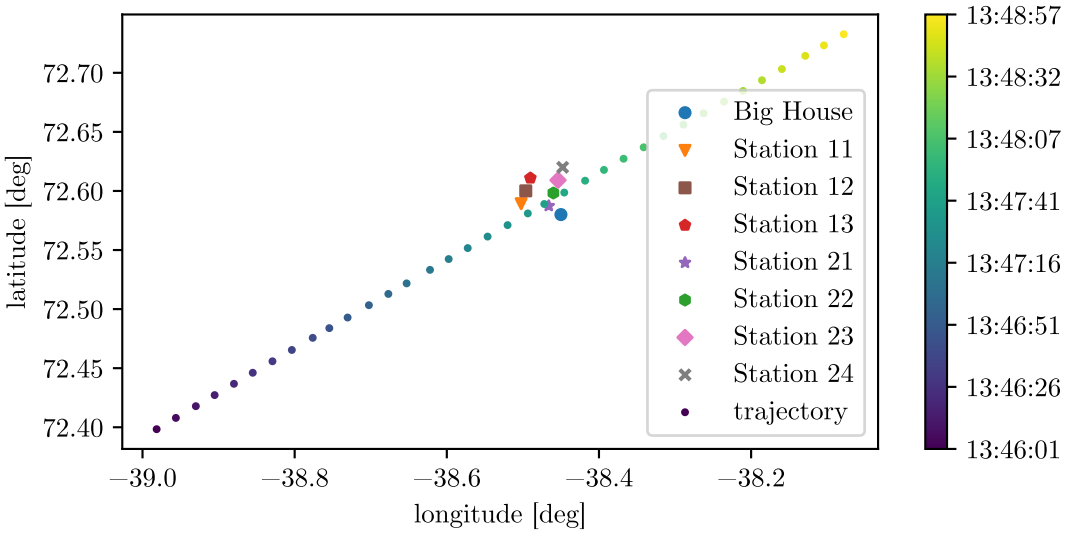

Figure 25: Flight CPA085 on 2023-05-07 flying directly over RNO-G in a straight line. Time is indicated by the colorbar.

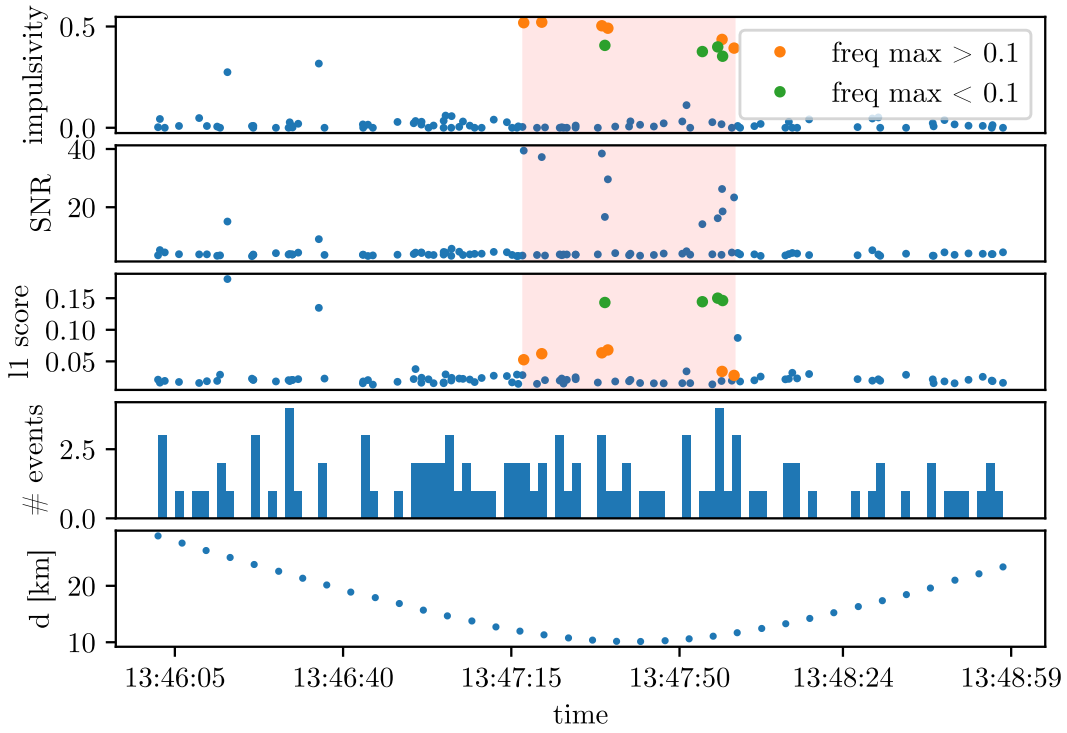

Figure 26: Scores for CPA085 on 2023-05-07. The scores are calculated based on the radiant trigger events seen in RNO-G for station 11 channel 13 (upward facing LPDA). The first 3 axes display impulsivity, SNR and L1 score over time. The fourth is a histogram of the trigger time. The fifth displays the 3D-distance of the plane to station 11. The marked region (red) is for events with high impulsivity. The colors (orange, green) indicate the two classes of events that can be observed. In the frequency spectrum (Figure 27) one has the main peak below and the other one above 0.1 [GHz].

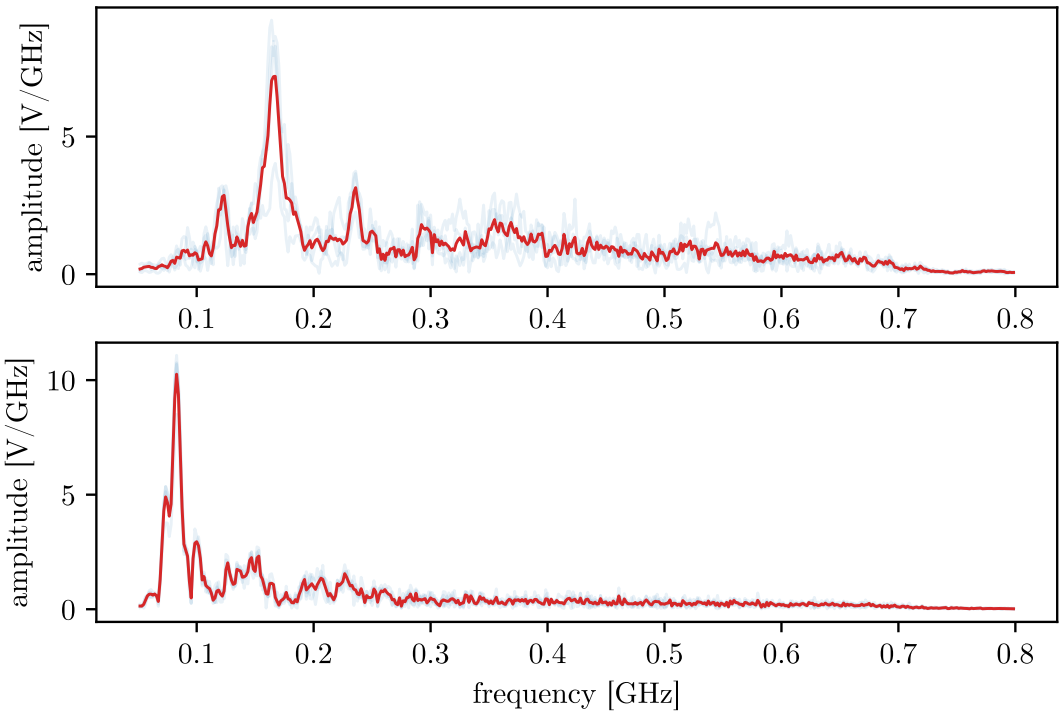

Figure 27: Mean spectra for flight CPA Figure 26. Two event categories could be seen in SNR (marked region). The spectra with in blue with low alpha were plotted. The mean spectra were plotted on top in red. The spectrum on top is from the category of events with max_freq > 0.1 [GHz], the lower spectrum for events with max_freq $<$ 0.1 [GHz]. Both event types have a distinctive peak but consist of a broad range of frequencies.

5 Investigation of a potential decline in trigger−rate with increasing distance of airplanes

In this section the correlation between airplane distance and the trigger−rates in RNO-G is investigated. First the assumption, based on which a decline in trigger−rate for higher distances, from plane to detector, is expected, gets explained. Then technical details in the preparation of used data are discussed. The main challenges are discussed. Finally the average trigger−rate for all flights and afterwards for JAL flights only are shown.

5.1 Initial assumption

In this section the influence of nearby planes on the trigger−rate is investigated. The basic assumption is that airplane signals can not reach the detector from infinitely far away. Due to attenuation, reflection and refraction the signal strength is assumed to decline over time, therefore distant signals will not trigger events in the detector anymore. Spherical waves will decline with $\frac{1}{r^2}$ even in vacuum. Based on this assumption one expects a decline in trigger−rate for higher distances as it could be observed for Skier31 in Figure 20. Airliners, unlike skiers, do not emit a continuous stream of signals, rather spontaneous emission, at random positions, could be observed. In a large enough data set consisting of airplane signals only, there should however still be a pile up in the average trigger−rate for lower distances, that declines for d $\rightarrow \infty$, when looking at airliners. Seeing such a behaviour can give interesting insights in airplane background detection.

There are a few steps that have been done in order to produce a dataset for the analysis. Foremost all flight tracker data from 2022-06-01 till 2022-11-01 was collected. The year 2022 was chosen because detector data from 2022 is unblinded, meaning all information is free to use in analysis. For blinded data only the trigger−times and around 3-5% of the traces, that get chosen randomly can be used. Trace information is however needed in order to make cuts on the data. In an unfiltered data set airplane signals would most likely be overwhelmed by other backgrounds and noise. Making cuts on the data, helps reducing backgrounds and noise. A cut on impulsivity > 0.3 e.g. filters out all thermal noise and most of cw.
The invetigated time interval gets reduced by the time the stations were not taking data. Due to maintenance work and lack of power supply in winter the stations do not run all year. The availability of data for station 11, for flight times, can be seen in Figure 28.

5.2 Data preparation

Before combining FlightTracker data with detector events some flights were taken out. Skiers were excluded from the analysis. With skiers there often times comes noise from ground activities (walkietalkies, snowmobiles etc.) and this may introduce unwanted artifacts in the analysis.
N/A flights were taken out.
Airplanes that fly the same routes twice a day were excluded. The way that flight duration is calculated in the code is by taking the first and last datapoint in a certain radius around RNO-G for a given day. If a plane flies a route with the same

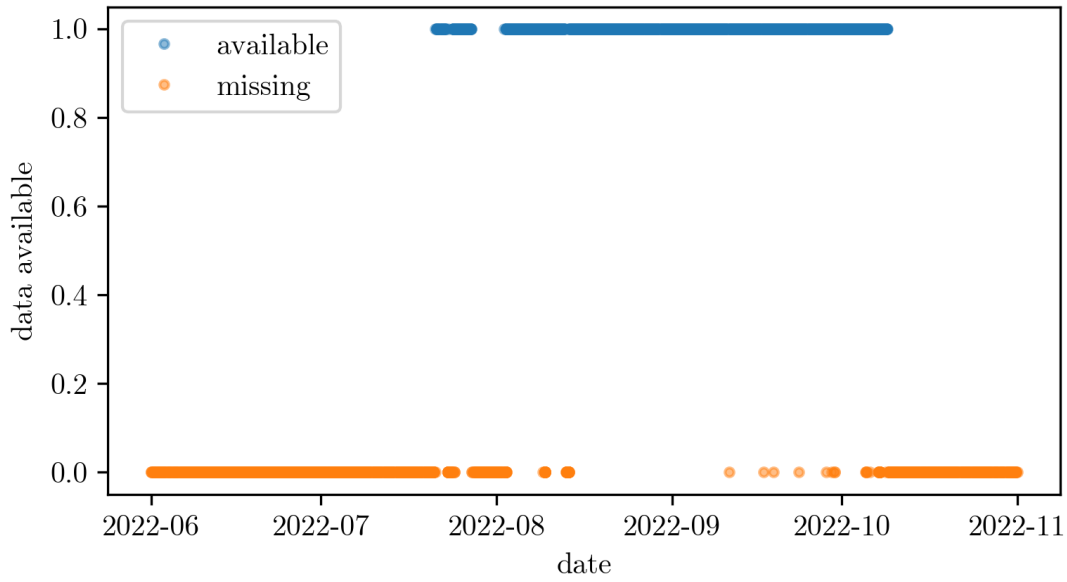

Figure 28: Times in which station 11 in RNO-G took data in 2022 are shown in blue. Downtimes are shown in orange.

flightnumber−hexcode combination twice in one day, a wrong duration gets calculated, eventually leading to problems. As this happened for only 19 flights they were simply excluded from the data.
Force−triggers were excluded from the detector data as they do not bring added value. In the next step detector and flight tracker data get combined. For each flight all events that happened during the flight are joined. The trigger−rate is calculated based on the trigger−times with a binning of 1 second. So for every full second the number of events during that second is counted. Now one wants to know the current distance of the plane. As ADS-B data and therefore distance information gets logged with 0.2 Hz, there only is a data point every 5 seconds. Therefore the distance for each full second gets linearly interpolated from the flight tracker data. Due to the planes traveling in relatively straight lines, the error is low. Skiers that sometimes fly in circles get excluded from the analysis anyways.
Afterwards all flights get joined and every full second with multiple flights gets dropped, in order to avoid counting events twice. Therefore some trajectories are only contained partially.

5.3 Choice of presentation and challenges

In order to make a potential decline in trigger−rate visible different ways of presenting the data were investigated. One candidate is a 2D-histogram, where trigger−rate over distance gets plotted. The main challenge however is that a 2D-histogram is not normalized. The containment area around RNO-G grows quadratically with the radius and therefore more flight tracker datapoints are contained for higher distances. Also the

histogram of flight tracker datapoints for a single flight has a sharp peak for minimal distance. This effect is caused by the geometry of the problem.
Let a plane fly in a straight line with constant velocity v = const. and constant altitude z = const., then the radius r is given by $r = \sqrt{x^2 + y^2 + z^2}$. One can choose a coordinate system with x' and y' so that y' = const. and x' is on the trajectory. Therefore $r = \sqrt{x'^2 + z^2}$. For $x' >> z : r \simeq x'$ and $\frac{dr}{dx} \simeq 1$ For $x' << z : r \simeq z$ and $\frac{dr}{dx} \simeq 0$. This means the rate of change in radius with x is not constant but rather varies with x. As the rate of change in x is constant, the time spent in each distance bin is longer for low distances. This can be seen in Figure 29.
The length travelled in each bin can be derived from the Pythagorean theorem:

$$
\begin{aligned}
L_1 &= 2 \cdot \left(\sqrt{(R + \mathrm{k})^2 - R^2} \right) \\
L_2 &= 2 \cdot \left(\sqrt{(R + 2 \cdot \mathrm{k})^2 - R^2} - L_1 \right) \\
&\ldots \\
L_n &= 2 \cdot \left(\sqrt{(R + n \cdot \mathrm{k})^2 - R^2} - \sum_{i=1}^{n-1} L_i \right) \\
L_n &= 2 \cdot \left(\sqrt{(R + n \cdot \mathrm{k})^2 - R^2} - \sqrt{(R + (n-1) \cdot \mathrm{k})^2 - R^2} \right)
\end{aligned}
$$

Where R is the minimal radius from station to plane and k is the bin−size. In this illustration the bin−size is chosen so that it aligns perfectly with R, in reality this will not always be the case, therefore one will get a lower count in the first bin.

This accumulation of datapoints for small radii is illustrated in a histogram with much smaller bins in order to get a smooth looking curve Figure 30.

A way to avoid dealing with this is to calculate the average trigger−rate for every distance bin. Averaging for each distance comes with a normalization as the average is given by

$$\mathrm{avg(x)} = \frac{1}{N} \sum_{i=0}^{N-1} x_i$$

Therefore the number N of datapoints for each distance bin can differ, without impacting the average trigger−rate.

5.4 Average trigger−rate for all flights

Due to low statistics below 11 km and above 100 km those distances are taken out of the subsequent analysis.

When plotting the average trigger−rate over the distance for every flight that is contained in the data set (Figure 31) there is a visible increase of trigger−rate for distances up to $\sim$ 30 km. This however is not due to the trigger−rate actually being higher for lower distances but rather has to do with the different airliners that can be seen in the data subsets for different distances. Flights of JAL and ANA do mostly fly

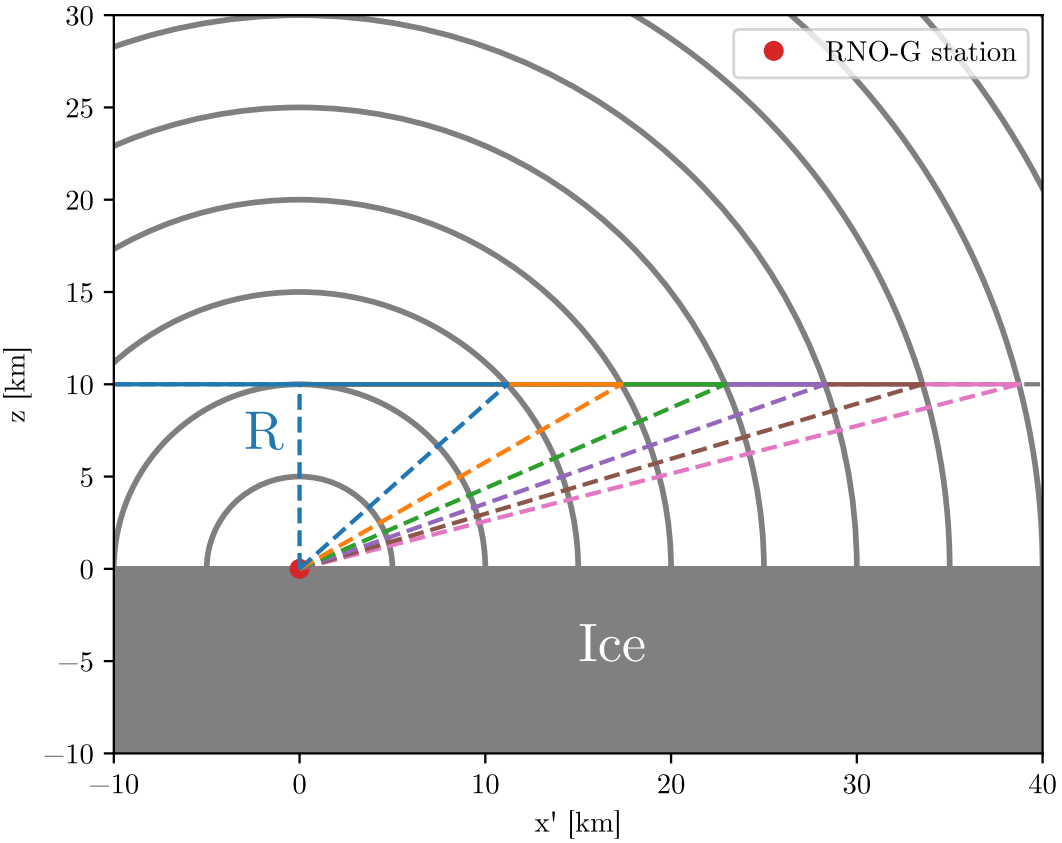

Figure 29: Depiction of a plane flying over a single station in RNO-G in a straight line. The length travelled in each distance bin, depicted by the gray circles, varies with the distance from plane to station. R is the minimal distance from plane to station.

directly over RNO-G, the other airlines mostly take routes a little bit further away. So when looking at distances from 10 km to 30 km the dataset is dominated by JAL and ANA (Figure 34). Different airlines do fly at different daytimes, depending on their start and destination (Figure 33). During the course of the day different backgrounds and noise sources are visible, leading to daytime dependent trigger−rates. Therefore the increase in trigger−rate seen for d $<$ 30 km is due to the average trigger−rate during the daytime of JAL and ANA differing from the average trigger−rate of the other airlines.
A simple proof can be obtained when shifting the detector data by a small time interval like 30 min. So instead of joining the events that happened in RNO-G during the course of a flight, one simply joins the events that happened 30 mins afterwards. These events are completely uncorrelated to the airplanes they get compared to. Doing so produces almost the same function, as can be seen in Figure 32. Most importantly the feature for small distances is still there, this is a clear indication that it has to be of other origin than the actual trigger−rate being higher for small d.

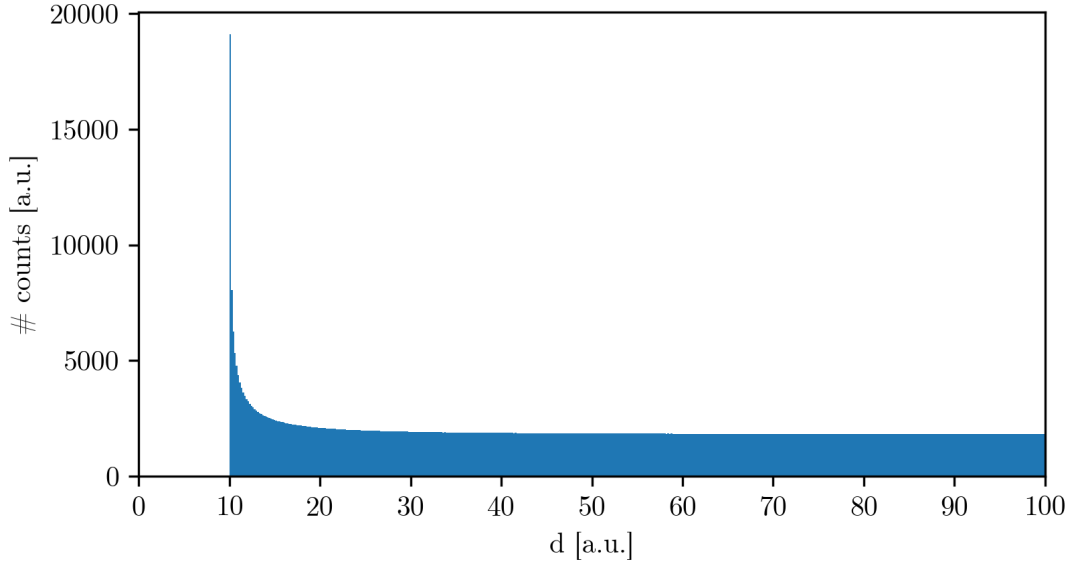

Figure 30: Histogram of the distance from the origin to a plane, which travels in a straight line in the x−y−plane, with a constant offset in z. The datapoints are taken with a constant rate. The histogram has a accumulation of datapoints for low d.

5.5 Average trigger−rate for JAL flights

In order to continue an analysis on a dataset with multiple airlines one would have to somehow normalize data with the average trigger−rates during different daytimes. This has to be investigated further. An easier approach is to restrict the analysis to JAL flights between 9 AM to 11 AM. This limits the impact of daytime dependent influences. Doing so produces a dataset with 156 JAL flights.

There is no visible decline in the average trigger−rate for JAL flights only. There is no decline over the whole distance and also no increase for lower distances. The radiant trigger−rate fluctuates around 0.6 Hz. The low threshold triggers fluctuate around 0.175 Hz. The assumption is that the increase in trigger−rate caused by airplanes is neglectable compared to other backgrounds and noise.
It could, in theory, be possible that the maximal distance of 100 km was chosen too low and airplane signals are getting detected equally distributed over all distances. This is assumed not to be the case, as skiers could only be seen for distances much lower.

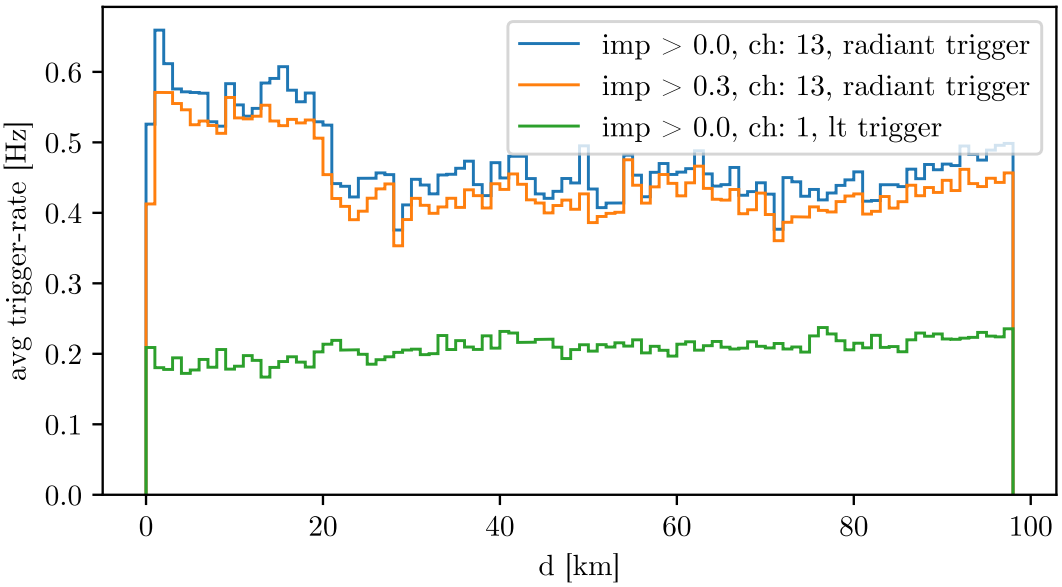

Figure 31: Average trigger−rate calculated as a function of plane distance (3D) for all planes in station 11 in the time interval mentioned above. Radiant triggers are shown with different cuts on impulsivity in channel 13. Low threshold (lt) triggers are shown without cuts in channel 1.

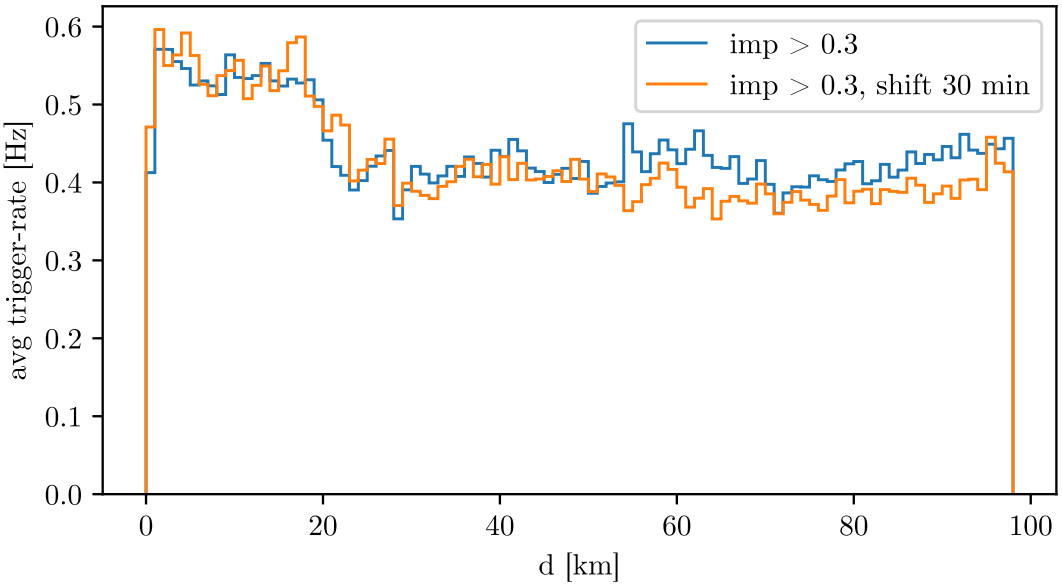

Figure 32: Average trigger−rate as a function of plane distance for all planes in station 11, radiant triggers, with a cut on impulsivity > 0.3 in channel 13. The actual trigger−rate is plotted as well as the trigger−rate calculated by detector data 30 mins after each flight. The trigger−rate with shift is completely uncorrelated to the airplanes seen at RNO-G, therefore the increase in trigger−rate for d < 30 km has to be a feature of other origin than airplane signals.

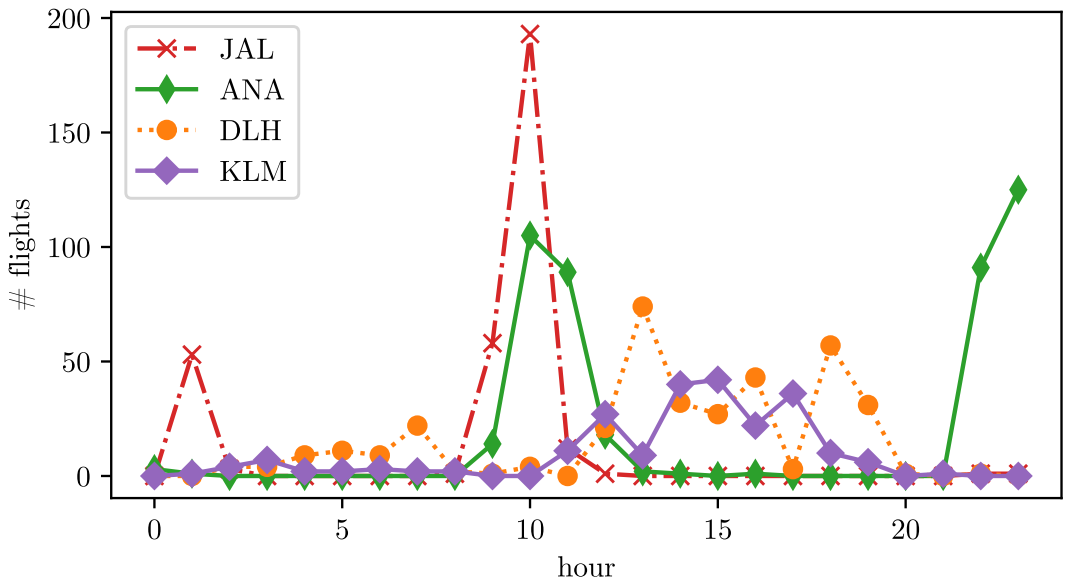

Figure 33: Hour of the day when different airlines are seen at RNO-G from 2022-07 to 2022-11. Only the top 4 most common airlines are plotted. Flights of JAL and ANA have nearly no overlap with DLH and KLM.

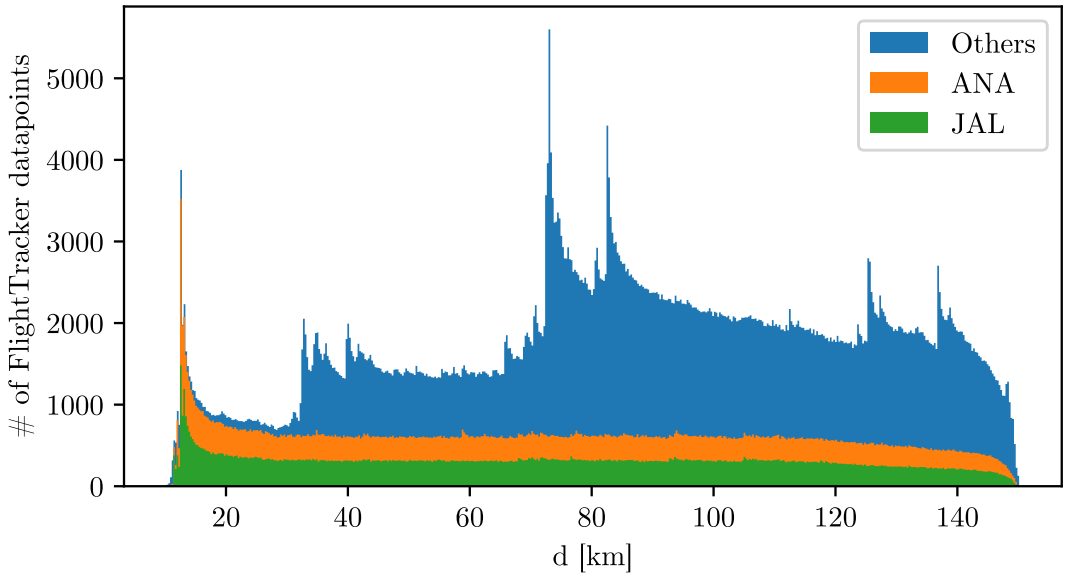

Figure 34: Stacked histogram of the contribution of FlightTracker datapoints to Figure 31. The histograms for JAL, ANA and all others are stacked upon each other. This is done to illustrate that the contribution to datapoints below a distance of 30 km is dominated by JAL and ANA flights.

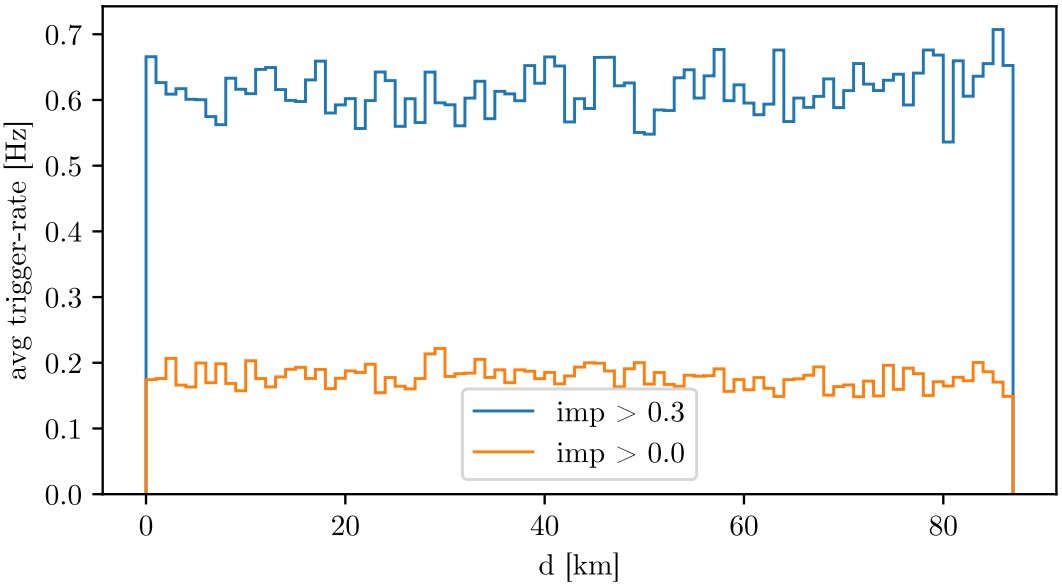

Figure 35: Average trigger−rate as a function of plane distance for JAL planes only, in station 11. Radiant triggers are shown with a cut on impulsivity in channel 13. Low threshold (lt) triggers are shown without a cut in channel 1.

6 Summary

Airplanes can be seen at RNO-G throughout the whole year. On average there are multiple airplanes per day passing RNO-G. The numbers do vary a lot from day to day and over the years. Skiers can only be seen during summer time. Commercial aircrafts, even from different airlines, do often take the exact same routes. So there are routes that get used quite frequently and others were there are barely any flights. The normal airliner flies at around 10 km height. Planes from the two japanese airlines JAL and ANA, most of the time, do fly a path that goes exactly above RNO-G. Sometimes they fly north of that standard route, but never south.
Almost all skiers that were seen proceeded to land at the skiway. Before that they usually circle RNO-G at least once. During their approach they fly at around 3 km altitude, lowering as they proceed to land.
When looking at the signals emitted by planes there is a clear distinction between skiers and airliners. Skiers are very noisy and for a radius of $\sim$ 10 km a clear correlation between the signal strength and the distance from plane to RNO-G can be observed. Different types of signals are seen simultaneously, most likely stemming from different sources. The propeller engines are suspected to be one source of noise. Also the presence of skiers usually goes along with ground activity, therefore a lot of communication (cw) can usually be observed.
Airliners do also emit RF signals. There is no clear correlation between a jet airplane's distance and the signals emitted. Rather there seems to be spontaneous signal emission. If the jet engines themselves emit noise in the RF regime is unknown. As no distance−dependent rise in trigger−rate or signal strength could be observed, the jet engines cannot be too noisy.

Methods of analysing signals measured by RNO-G are discussed. 3 different scores are introduced that help to differentiate between different kinds of signals. Airplane signals are assumed to be mostly short and impulsive. This is also the type of signal one would use for calibration, therefore it is important to be able to extract those from all signals.

The average trigger−rate over the distances of airplanes was plotted. The trigger−rate seems to be completely uncorrelated of the aircrafts distances however. The analysis was done by looking at events seen by RNO-G during times airplanes were closer than 150 km (3D) to the array. The initial assumption is that for a large enough distances signals are not able to reach RNO-G anymore. Either because they are too weak or because of total reflection on the ice surface due to a small zenith angle. The reason one was not able to see such a cut−off distance is most likely that the data sample used for analysis is dominated by other backgrounds.

7 Conclusion

This thesis wanted to answer, to what extend there is airplane induced background at RNO-G and if it is possible to tag airplane signals. Either to reduce background in neutrino analysis or to utilize them for calibration. Software was developed that helps with the analysis. A python code was written that gives information about any flights present, in a variable containment radius around RNO-G, at any time.
Few airplanes, that emitted RF signals, which were seen by RNO-G, were already known. It was however unknown how much airtraffic there is and if RF signals would be emitted frequently. The thesis gives an overview of airtraffic and the abundance of different types of airplanes. The main flight routes are identified and airlines that behave strangely were found.
The attempt of tagging airplanes was done based on trigger−rates of the stations in RNO-G, as for some of the known flights trigger−rates were influenced heavily by emitted RF signals. An increase in trigger−rate could however not be found when averaging over many flights. Possible explanations are, that few airplanes do emit RF noise in the first place. The signals emitted, even after cutting on impulsivity, are dominated by other backgrounds in RNO-G. Airplane tagging based on trigger−rates therefore does not seem to be a valid option. Possible strategies for identifying airplanes in the future are discussed in section 8.

8 Outlook

This section will discuss some ideas and technical details for future plane analysis at RNO-G, that were outside the scope of this bachelors thesis.

The approach of finding airplane signals in RNO-G in this thesis was based on trigger−rates in the detector. As shown airplanes are not noisy enough to identify them based on trigger−rates in a data sample with other backgrounds. Even if only potential airplane signals are filtered out by cutting on impulsivity. One of the main challenges for the future will therefore be to find another way of identifying airplanes in the detector data. To do so a better understanding of the appearance of airplane noise is needed. One approach is creating a catalog of pure airplane signals.
This is not trivial. To ensure that an event stems from an airplane one has to reconstruct the arrival direction and compare it with airplane positions recorded by the flight tracker. This can be done by arrival−time comparison of signals in different antennas. Under the assumption that signals are plane waves originating at infinite distance, it is possible to reconstruct the arrival direction, when signals are seen in at least 3 antennas. Usually the 3 upward−facing LPDAs are best for reconstruction of signals from above. However, not always can signals be seen in all 3 antennas, and even if so, it is not trivial to determine their exact timing differences due to slightly different signal shapes in different channels.
As this process is very calculation intensive it does make sense to have a set of potential candidate events instead of performing a direction−reconstruction for every event. One way of producing such a set is by looking at coincident events in multiple stations. When different stations see an event in a small coincidence−window it can still be unrelated

events, but the chance of finding non−local background source is higher. Noise from the stations itself, e.g. wind, LoRaWAN or solar−panel charging noise is only seen in the station it gets produced. Signals from up in the sky are more likely to be seen in multiple stations, if they are strong enough.

When looking at coincident events in at least 3 stations in a coincidence window of 10 μs from 2022-06-15 till 2022-09-15, there are 2870 clusters of events. For 88 % of those a flight (46 % skiers) was found nearer than 50 km (3D) to the array. For a radius of 10 km (3D) still 43% (all skiers) of the time airplanes were nearby. This is much more than the 7 % planes, that are nearer 50 km when looking at all time.
When creating such a sample of supposedly pure airplane signals it does also make sense to store the frequency spectra. Having a catalog of different signal types helps with finding distinct sources of noise on planes. Also it allows for training a neural network (e.g. variational auto−encoder VAE) to distinguish between and find such events in the future.

The tools developed for this thesis can help with future analysis. Airplane position, zenith, azimuth angles and other information can easily be obtained for a given time period. These infomation can be compared to reconstructed signal directions and help validating analysis.
If one is able to create a pure sample of airplane noise in the future, the trigger−rate over distance analysis can be repeated, in order to determine the containment area for airplane signals at RNO-G.

Bibliography

[1] A. Aab et al. „Nanosecond-level time synchronization of autonomous radio detector stations for extensive air showers“. In: *JINST* 11.01 (2016), P01018. DOI: 10.1088/1748-0221/11/01/P01018. arXiv: 1512.02216 [physics.ins-det].

[2] S. Agarwal et al. „Solar flare observations with the Radio Neutrino Observatory Greenland (RNO-G)“. In: *Astropart. Phys.* 164 (2025), p. 103024. DOI: 10.1016/j.astropartphys.2024.103024. arXiv: 2404.14995 [astro-ph.SR].

[3] J. A. Aguilar et al. „Design and Sensitivity of the Radio Neutrino Observatory in Greenland (RNO-G)“. In: *JINST* 16.03 (2021). [Erratum: JINST 18, E03001 (2023)], P03025. DOI: 10.1088/1748-0221/16/03/P03025. arXiv: 2010.12279 [astro-ph.IM].

[4] M. Aker et al. „Direct neutrino-mass measurement with sub-electronvolt sensitivity“. In: *Nature Phys.* 18.2 (2022), pp. 160–166. DOI: 10.1038/s41567-021-01463-1. arXiv: 2105.08533 [hep-ex].

[5] G. A. Askar'yan. „Excess negative charge of an electron-photon shower and its coherent radio emission“. In: *Zh. Eksp. Teor. Fiz.* 41 (1961), pp. 616–618.

[6] S. W. Barwick et al. „Radio detection of air showers with the ARIANNA experiment on the Ross Ice Shelf“. In: *Astropart. Phys.* 90 (2017), pp. 50–68. DOI: 10.1016/j.astropartphys.2017.02.003. arXiv: 1612.04473 [astro-ph.IM].

[7] W. Blythe, H. Anderson, and N. King. *ADS-B Implementation and Operations Guidance Document*. International Civil Aviation Organization, 2011.

[8] The University of Chicago. *RNO-G Flight Tracker*. Accessed: 2024-09-01. 2024. URL: https://rno-g.uchicago.edu/data/flight-tracker/.

[9] Cosmin Deaconu. personal correspondence. 2024.

[10] FlightAware. *JAL44 Flight History: EGLL to RJTT on September 6, 2024*. https://de.flightaware.com/live/flight/JAL44/history/20240906/1830Z/EGLL/RJTT. Accessed: 2024-09-08. 2024.

[11] Aviation Hunt. *Aircraft Antennas and Probes*. Accessed: 2024-09-01. 2024. URL: https://www.aviationhunt.com/aircraft-antennas-and-probes/.

[12] Oliver Jowett. *dump1090-mutability*. GitHub repository. Accessed: 2024-08-18. 2024. URL: https://github.com/adsb-related-code/dump1090-mutability/blob/master/README-json.md?plain=1.

[13] P. Laub. „Machine-Learning-based Background Identification for the Radio Neutrino Observatory Greenland“. Master's Thesis. 2024. URL: https://ecap.nat.fau.de/wp-content/uploads/2024/01/Master_thesis_final_Philipp_Laub.pdf.

[14] L. Pyras, C. Glaser, S. Hallmann, and A. Nelles. „Ultra-high energy muons in radio neutrino detectors“. In: *PoS* ICRC2023 (2023), p. 1076. DOI: 10.22323/1.444.1076.

[15] RNO-G Collaboration. *RNO-G Calibration Meeting*. https://radio.uchicago.edu/wiki/images/1/14/RNO-G_calibration_meeting_2024-03-20_Trigger_Time_Clustering.pdf. Accessed: 2024-09-06. 2024.

[16] Junzi Sun. *ADS-B Basics*. Accessed: 2024-08-24. 2021. URL: https://mode-s.org/decode/content/ads-b/1-basics.html.

Appendix

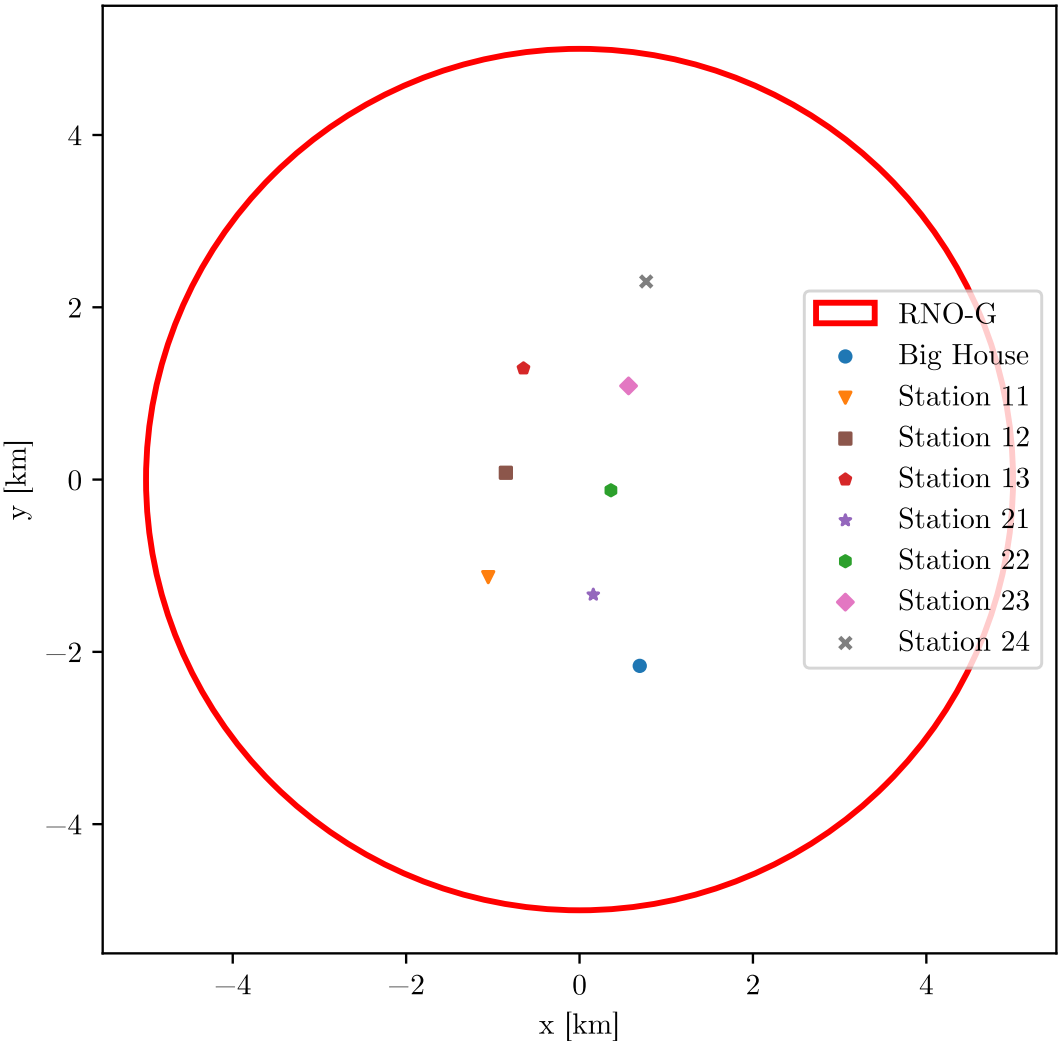

Figure 42: Stations in RNO-G contained in the red circle used in Trajectory plots in section 3

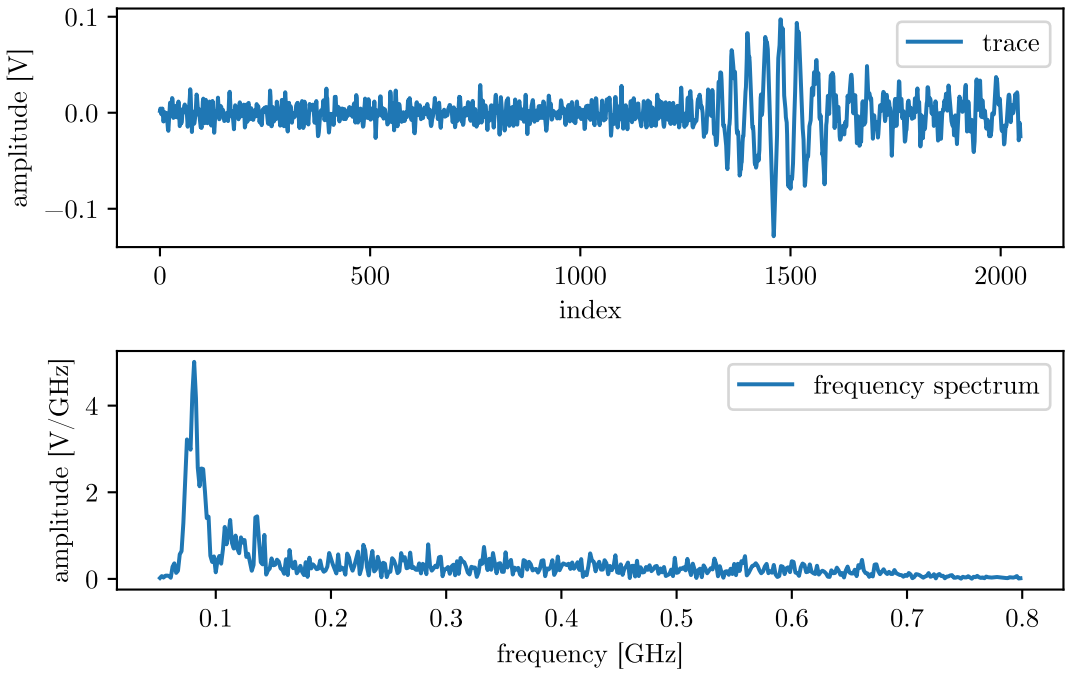

Figure 36: Example event measured in RNO-G.
Station Nr.: 11, Run Nr.: 1313, Event Nr.: 1980, Channel Nr.: 13.
The event is contained in the marked region, with $10 < \text{SNR} < 50$, in Figure 20.
Top: The antenna voltage is shown over the index representing a whole trace with 2048 data points, over a duration of 640 ns.
Bottom: The frequency spectrum of the signal is shown from 50 MHz to 800 MHz.A dominant peak can be seen for $\sim$ 80 MHz.

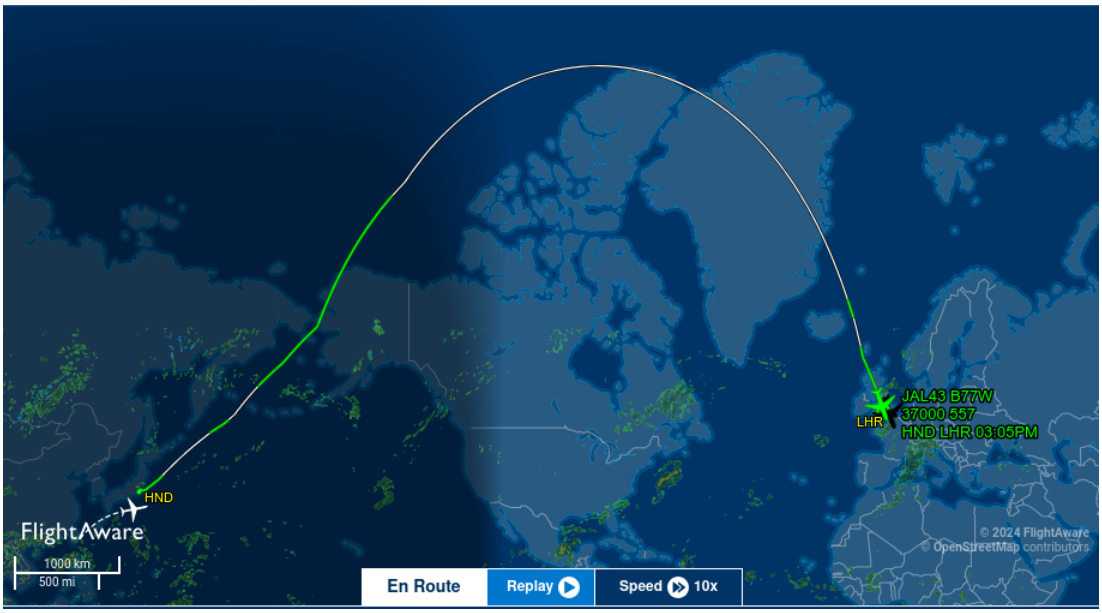

Figure 43: Trajectory of flight JAL43 on 2024-09-06 (Tokio Int'l (Haneda) – London Heathrow) as seen by [10]. This flight took the route over greenland.

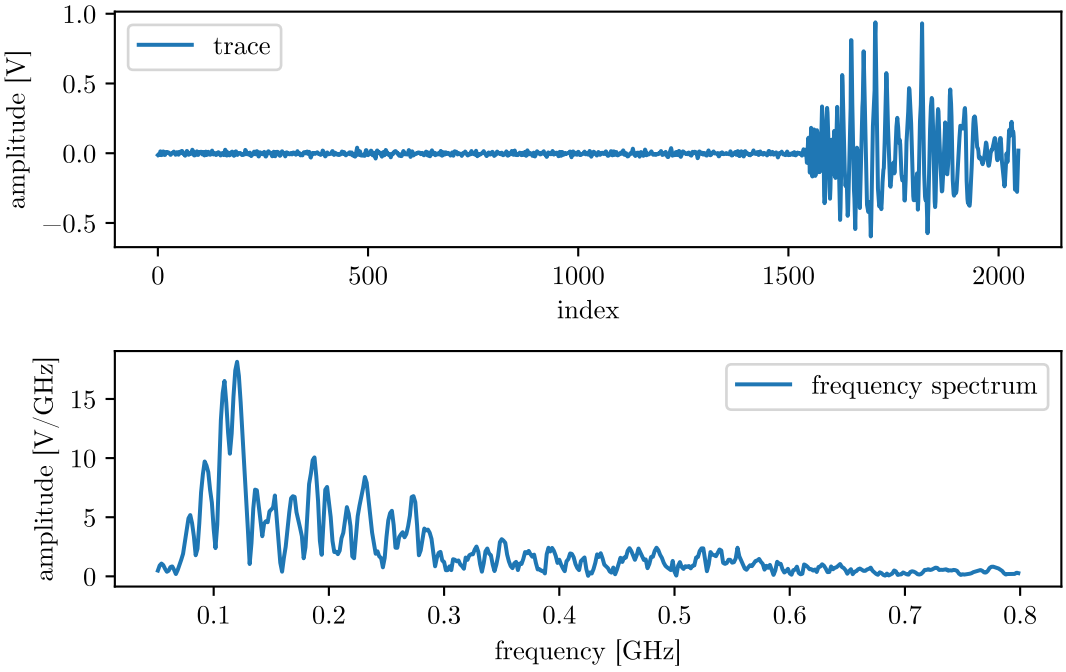

Figure 37: Example event measured in RNO-G.
Station Nr.: 11, Run Nr.: 1313, Event Nr.: 1954, Channel Nr.: 13.
The event is contained in the marked region, with $50 < \text{SNR} < 100$, in Figure 20.
Top: The antenna voltage is shown over the index representing a whole trace with 2048 data points, over a duration of 640 ns.
Bottom: The frequency spectrum of the signal is shown from 50 MHz to 800 MHz. A broad range of peaks can be seen from 50 MHz to 300 MHz.

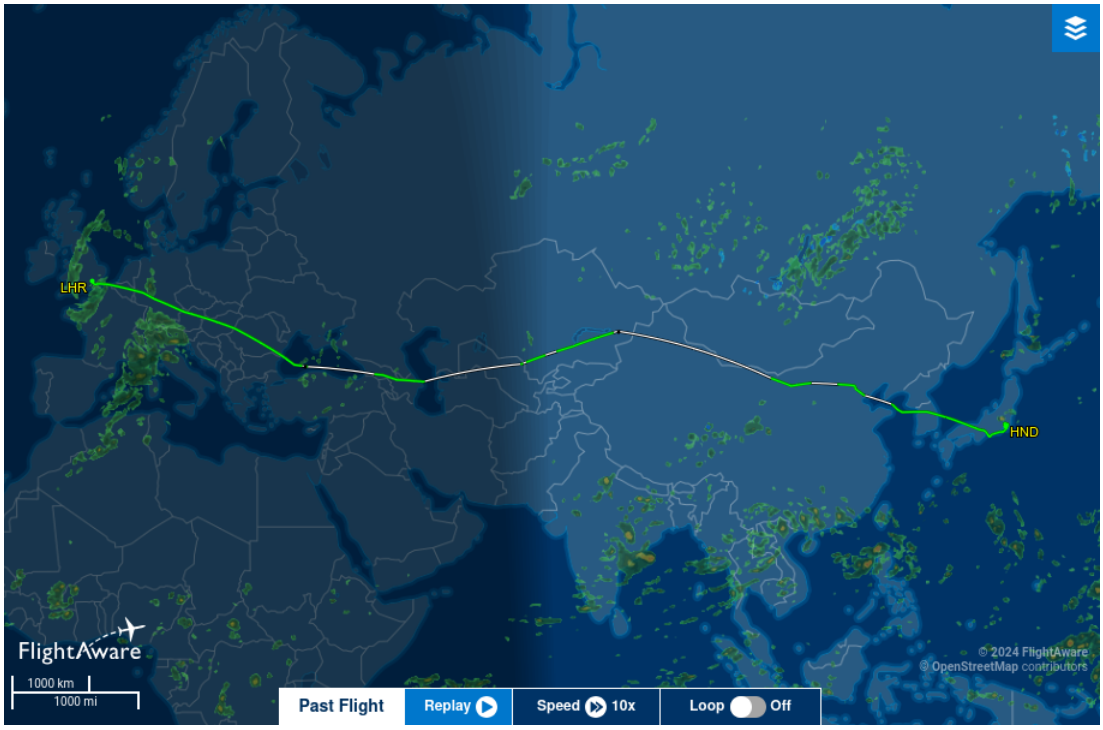

Figure 44: Trajectory of flight JAL44 on 2024-09-07 (London Heathrow – Tokio Int'l (Haneda)) as seen by [10]. This flight did not take the route over greenland.

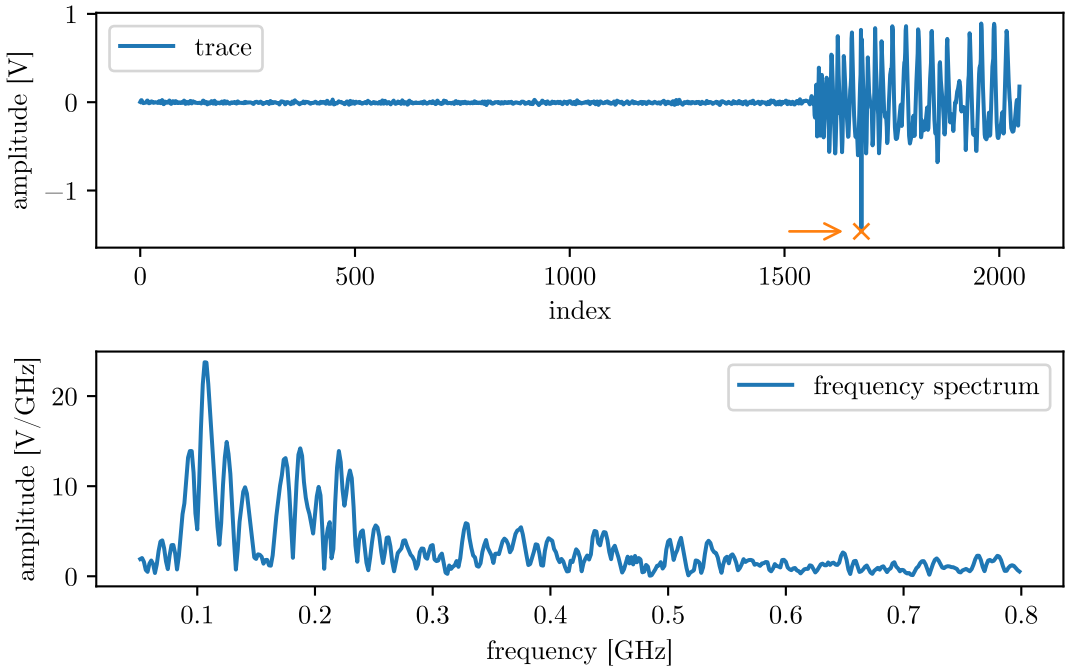

Figure 38: Example event measured in RNO-G.
Station Nr.: 11, Run Nr.: 1313, Event Nr.: 2247, Channel Nr.: 13.
The event is contained in the marked region, with 100 < SNR, in Figure 20.
Top: The antenna voltage is shown over the index representing a whole trace with 2048 data points, over a duration of 640 ns.
Bottom: The frequency spectrum of the signal is shown from 50 MHz to 800 MHz. The frequency spectrum looks similar to the one shown in Figure 8

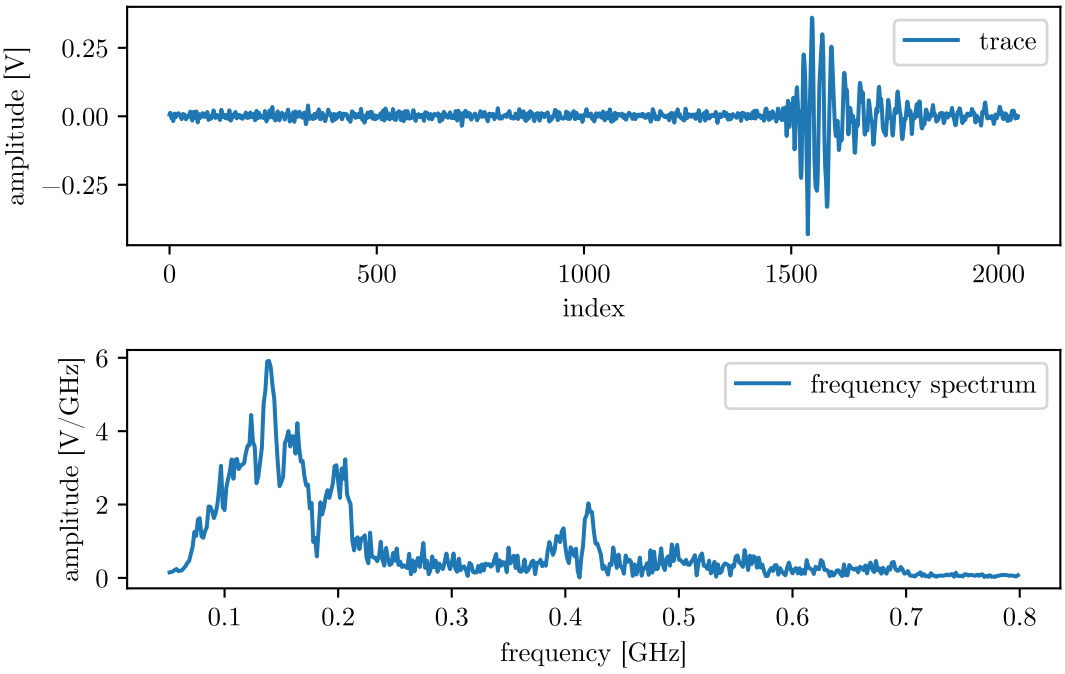

Figure 39: Example event measured in RNO-G.
Station Nr.: 11, Run Nr.: 1239, Event Nr.: 269, Channel Nr.: 13.
The event is contained in the marked region in Figure 23.
Top: The antenna voltage is shown over the index representing a whole trace with 2048 data points, over a duration of 640 ns.
Bottom: The frequency spectrum of the signal is shown from 50 MHz to 800 MHz.

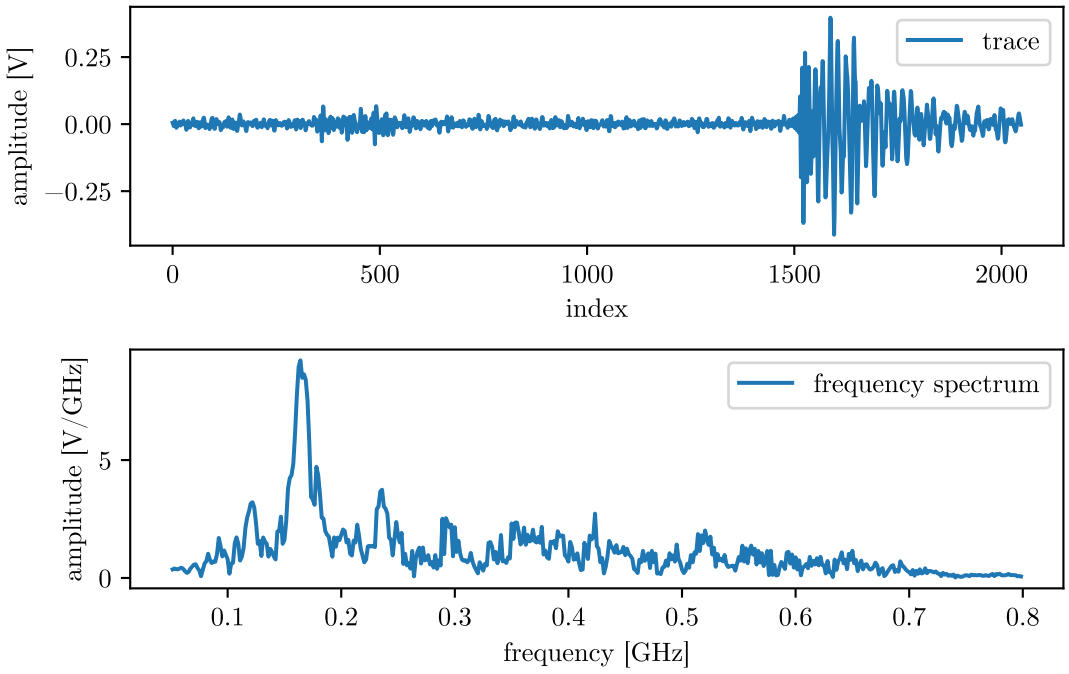

Figure 40: Example event measured in RNO-G.
Station Nr.: 11, Run Nr.: 2158, Event Nr.: 734, Channel Nr.: 13.
The event is contained in the marked region in Figure 26 with freq_max > 0.1 [GHz] .
Top: The antenna voltage is shown over the index representing a whole trace with 2048 data points, over a duration of 640 ns.
Bottom: The frequency spectrum of the signal is shown from 50 MHz to 800 MHz.

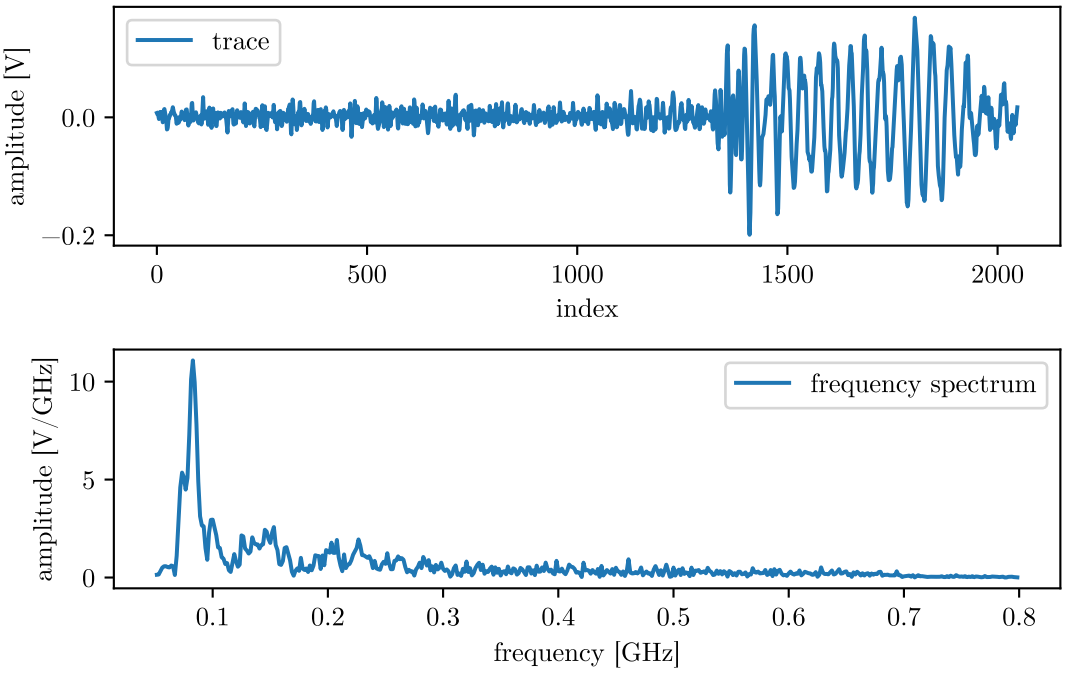

Figure 41: Example event measured in RNO-G.
Station Nr.: 11, Run Nr.: 2158, Event Nr.: 751, Channel Nr.: 13.
The event is contained in the marked region in Figure 26 with freq_max < 0.1 [GHz] .
Top: The antenna voltage is shown over the index representing a whole trace with 2048 data points, over a duration of 640 ns.
Bottom: The frequency spectrum of the signal is shown from 50 MHz to 800 MHz.

Eigenständigkeitserklärung

Hiermit versichere ich, Oliver Schlemper (22391326), die vorgelegte Arbeit selbstständig und ohne unzulässige Hilfe Dritter sowie ohne die Hinzuziehung nicht offengelegter und insbesondere nicht zugelassener Hilfsmittel angefertigt zu haben. Die Arbeit hat in gleicher oder ähnlicher Form noch keiner anderen Prüfungsbehörde vorgelegen und wurde auch von keiner anderen Prüfungsbehörde bereits als Teil einer Prüfung angenommen.

Die Stellen der Arbeit, die anderen Quellen im Wortlaut oder dem Sinn nach entnommen wurden, sind durch Angaben der Herkunft kenntlich gemacht. Dies gilt auch für Zeichnungen, Skizzen, bildliche Darstellungen sowie für Quellen aus dem Internet.

Mir ist insbesondere bewusst, dass die Nutzung künstlicher Intelligenz verboten ist, sofern diese nicht ausdrücklich als Hilfsmittel von dem Prüfungsleiter bzw. der Prüfungsleiterin zugelassen wurde. Dies gilt insbesondere für Chatbots (insbesondere ChatGPT) bzw. allgemein solche Programme, die anstelle meiner Person die Aufgabenstellung der Prüfung bzw. Teile derselben bearbeiten könnten.

Ort, Datum	Unterschrift